RELAXATION PROCESSES IN TERTIARY-BUTYL-PHTHALOCYANINE IN SHPOL'SKII MATRICES AT LOW TEMPERATURES

by

Jialiang Gao

BSc. Gaungzhou Teacher's College, 1986

THESIS SUBMITTED IN PARTIAL FULFILLMENT OF

THE REQUIREMENTS FOR THE DEGREE OF

Master of Science

in the Department

of

Physics

SIMON FRASER UNIVERSITY

July 1992

Approval

Name: Jialiang Gao

Degree: Master of Science

Title of thesis: Relaxation Processes in Tertiary-butyl-phthalocyanine in Shpol'skii Matrices at Low Temperatures

Examining Committee:

Chair: Dr. S. P. Watkins

Dr. K. E. Rieckhoff
Senior Supervisor, Professor
Department of Physics

Dr. E-M. Voigt
Senior Supervisor, Professor
Departments of Physics and Chemistry

Dr. S. R. Morrison
Supervisor, Professor
Department of Physics

Dr. R. F. Frindt
University Examiner
Department of Physics
Simon Fraser University

Date of Approval August 13, 1992

PARTIAL COPYRIGHT LICENSE

Title of Thesis/Project/Extended Essay

RELAXATION PROCESSES IN TERTIARY-BUTYL-PHTHALOCYANINE IN SHPOL'SKII MATRICES AT LOW TEMPERATURES

Author: _____
(signature)

Jialiang Gao
(name)

Aug 19, 1992
(date)

Abstract

Free base tetra-tertiary-butylphthalocyanine(TBH_2Pc) is a pigment with molecular weight of 736. In many aspects it is similar to its parent compound porphyrin, which plays an important role in electron transfer processes in nature. TBH_2Pc can be dissolved in *n*-alkane and forms a solid matrix(Shpol'skii matrix) at low temperatures, which shows quasilinear fluorescence spectra. In slowly grown crystals the TBH_2Pc molecules occur in two orientations, which are co-planar and have their N-H axes at right angles, thus two tautomeric species can be distinguished.

In this thesis we first identify the most appropriate *n*-alkane solvent for TBH_2Pc by analyzing the fluorescence and excitation spectra and then report on the studies of two relaxation processes of TBH_2Pc. These processes can be seen by selectively exciting the molecule into the S_1 band and monitoring the time resolved $S_0 \leftarrow S_1$ fluorescence behavior. It is found that the transition between the lowest triplet state to the ground state singlet occurs in times of the order of milliseconds, while another process that lasts tens of seconds is a result of the proton tunnelling between the ground states of the two tautomeric species. A simplified three-level model and a more comprehensive WKB calculation are presented to explain these processes. The $S_0 \leftarrow T_1$ rate and proton tunnelling rate are experimentally determined to be $T = (14.3 \pm 0.8) s^{-1}$ and $S = (3.0 \pm 0.2) \times 10^{-2}\ s^{-1}$ respectively and the temperature dependence curve of the tunnelling rate is also given.

Acknowledgments

The author would like to thank Dr. K. E. Rieckhoff, Dr. E.-M. Voigt, senior supervisors, for their support and guidance in carrying out this study. He is also grateful to Dr. Wen H. Chen of National Chiao-Tung University, Taiwan, whose technical help and theoretical enlightenment became crucial to this project.

Special thanks go to Leslie Smith, who continually supports the author's study; and Helen Evans of Malaspina College, whose tireless teaching in English has been much beneficial to this writing.

Discussions, concerns and encouragement from the faculty, colleagues in the department of physics, as well as financial support from Simon Fraser University are also gratefully acknowledged.

Table of Contents

List of Tables

List of Figures

CHAPTER 1 INTRODUCTION

1.1 OPTICAL RELAXATION PROCESSES FOR IMPURITIES IN SOLIDS

Although spin relaxation in magnetic resonance spectroscopy was documented as early as 1948[1], relaxation processes in optical transitions could not easily be detected until the invention of the laser, which provided a tunable, coherent, high intensity light source for narrow band excitation. The difficulty is obvious, since the characteristic time of allowed optical transitions corresponds to the life time of molecular states, which is of the order of 10^{-8} seconds. The observation of this transient process must be performed within this time interval after the saturation source is switched off.

Szabo[2,3] took advantage of the long lifetime(in millisecond range) of the R_1 band of ruby to directly observe optical relaxation. Personov[4] and Rebane[5] and their coworkers discovered that if molecules or ions with an energy level intermediate between the levels probed by optical absorption were doped into a material, the lifetime of absorption saturation could be very long, even infinite, provided that the decay lifetime of the intermediate state into the ground state was very large. This is equivalent to burning a *hole* in the absorption band of the ion or molecule(the terminology of *hole* is borrowed from [1], since in both cases a hole corresponds to the lack of net absorption at specific frequency on absorption band).

The discovery of persistent spectral holes has opened a completely new field for researchers to probe the intrinsic properties of ions or molecules. For example, the static and dynamic properties of spectral holes contain a wealth of microscopic interaction information

of the host-guest system. To name a few: the kinetics and order of photoinduced processes[6-8], bottleneck lifetime[9-12], spectral diffusion[13-15], electric and magnetic field effects[16-18], etc. Of the special interest are the relaxation mechanisms. These relaxation mechanisms are conventionally be classified into two categories: non-photochemical and photochemical. Here we are only concerned with the latter, which usually involves some internal change in the guest ion or molecule itself. This may include the photodecomposition[19-22], hydrogen bond rearragements[23,24], photoionization and trapping[25-27] and proton tautomerization(switching motion of the inner protons in porphyrin-like molecules)[5,6,12,15,28,29]. The latter is light induced tautomerization of the pair of central protons in porphyrin-like molecules. In this sense, free base porphyrins and phthalocyanines and their derivatives can be viewed as bistable devices, in that either of the two tautomers can be stable at low temperatures and light(or heat) can induce transformations between the two forms.

The purpose of this thesis is to investigate the relaxation processes of one of the derivatives of phthalocyanine, TBH_2Pc(tetra-tertiary butylphthalocyanine) in crystalline Shpol'skii matrices. Although hole-burning has been proven to be one of the most powerful techniques to study relaxation processes, we took advantage of the method of laser fluorescence spectroscopy to avoid certain technical difficulties in hole-burning experiments, such as the requirement of extremely narrow band lasers and sophisticated absorption apparatus. We report that proton tautomerization processes can be directly observed by monitoring the fluorescence intensity as a function of time after excitation; and the results report here show that some dynamic information similar to that from spectral hole-burning can be successfully acquired by this technique.

One of the fundamentals for the studies of relaxation process in host-guest system is that the electronic and vibrational transition details of the guest molecule must be fully

known, so that the coherent light source can selectively excite the guest molecule, and the luminescence signals can be precisely monitored. Unfortunately, as what will be made clear in the next section, spectral fine structures of the guest molecule, especially of the polyatomic organic compounds like TBH_2Pc, can not be obtained under ordinary conditions, as various mechanisms cause serious diffuseness of the spectra. Therefore, an intriguing question arises naturally: what special tactic should be used to eliminate(or at least to minimize) such broadening of the spectra? In order to answer this question, it is essential to review what is known about the spectra of molecules in solid solution.

1.2 GENERAL NATURES OF MOLECULAR SPECTRA IN SOLID SOLUTIONS

Molecules in solid solution are in many aspects very similar to impurity centers in crystals. Hence, we may take advantage of the main concepts of impurity center theory[30] to analyse molecular spectra. The nature of the spectrum of the impurity molecule is usually determined by electron-vibrational interactions of two types: interaction of the molecule's electrons with its intramolecular vibrations, usually referred to as vibronic coupling; and interaction with the intermolecular vibrations of the solid solvent, usually referred to as electron-phonon coupling. The vibronic coupling leads to a series of vibronic bands in the molecular spectrum along with the bands in the purely electronic transition region. However, contrary to those of the isolated molecules, the spectral features of impurities in solid are not only determined by vibronic coupling but also electron-phonon coupling. As is shown in figure 1.1, each vibronic band consists of a narrow zero-phonon line(ZPL), as result of transitions in the impurity molecule without any change in the phonon number of the solid solvent; and a broad phonon wing corresponding to those transitions of molecules with the simultaneous creation or annihilation of solvent phonons. The Debye-Waller factor, which is defined as

$$\alpha = \frac{I_{ZPL}}{I_{ZPL} + I_{PW}}, \tag{1.1}$$

where I_{ZPL} and I_{PW} are the integrated intensities of the zero phonon line and the phonon wing of the absorption respectively, not only depends strongly on the strength of the electron-phonon coupling, but also depends exponentially on temperature(see [31] for examples).

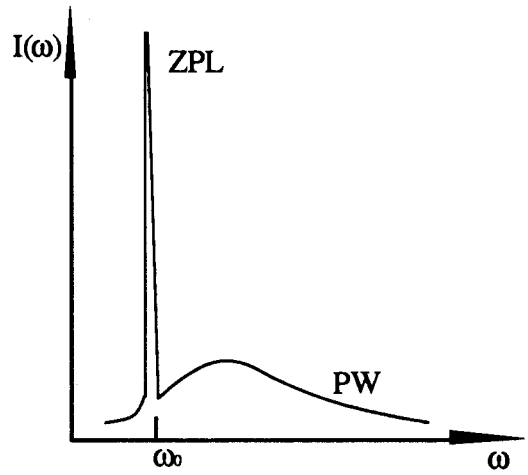

Fig.1.1 Typical spectral line of an impurity molecule in solid. It consists of a zero-phonon line(ZPL) and a broad phonon wing(PW). Only one vibronic band is shown.

Two extreme cases are considered here: (1) the electron-phonon coupling is strong ($\alpha \ll 1$). In such a case the intensity of zero phonon line is low even at very low temperatures. One- or multiphonon scattering cause wide phonon wings which smear out the the spectrum. (2) the electron-phonon coupling is weak and the phonon effect has been minimized. If we sufficiently lower the temperature, the Debye-Waller factor $\alpha \approx 1$(for one vibronic band), hence fine structure can sometimes be observed.

However, even at sufficiently low temperature and with weak electron-phonon coupling, inhomogeneous broadening still plays a decisive role[31-33], this is because the impurity centers in a real solid are situated in different local conditions. This can result in a

statistical distribution of the spectra that can spread hundreds of cm^{-1} in the frequency domain. As figure 1.2 shows a broad fluorescence profile is formed by a series of zero-phonon lines. This will usually be the case if the solid solvent is amorphous or quasi-amorphous rather than crystalline.

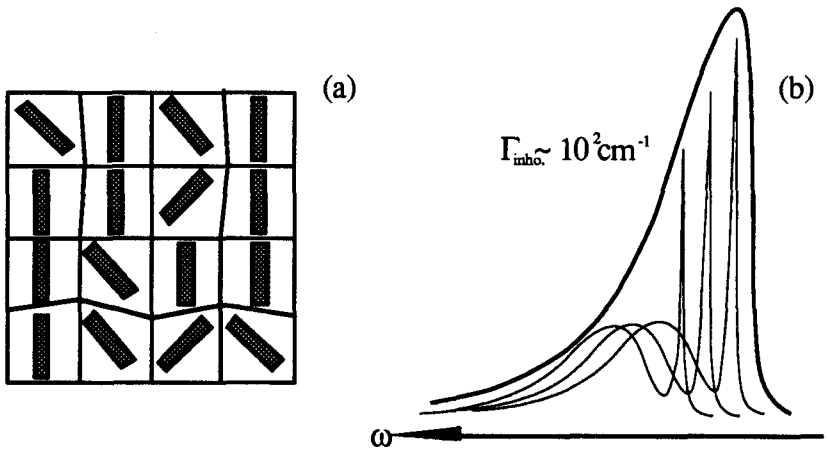

Figure 1.2 Inhomogeneous linewidth caused by local conditions of impurity centers. (a): scheme of guest molecule positions in real solid. (b): distribution of homogeneous fluorescence lines result in broad inhomogeneous envelope.

With the use of lasers, the aforesaid broadening in the fluorescence spectra can to a certain extent be eliminated by monochromatic excitation[34,35]. This is because if the monochromatic excitation frequency is that of a pure electronic or of the lowest vibronic transition, mainly those molecules that possess their absorption zero phonon lines at the laser frequency will undergo selective excitation. Then, in the emission spectrum, narrow lines belonging only to those molecules will appear, instead of a few broad bands.

However, monochromatic excitation is not a panacea for eliminating the inhomogeneous broadening in fluorescence spectra. The reason is that the "phonon wings" in figure 1.2 are not the purely phonon ones. If one considers more carefully, it can be

found that such a wing is a superposition of the true phonon wings of resonantly excited states and fluorescence bands(ZPL + PW) of those who are nonresonantly excited. In another words, these impurity centers are not excited only through zero phonon lines but also through the phonon wings. As we understand the width of the phonon wing is much wider than that of the zero phonon line, the number of nonresonantly excited centers can be large. Together they can make an appreciable contribution to the integrated intensity of the longwave wing(no longer called phonon wing) close to the fluorescence line and thus reduce the α. Theoretically it can be found[34] that the Debye-Waller factor α' in this case is between

$$\alpha^2 < \alpha' < \alpha \qquad (1.2)$$

and the specific value depends on excitation frequency and temperature.

Hence, in order to obtain the fluorescence fine structure of impurity centers in a solid, several aspects should be considered: temperature, monochromatic excitation, electron-phonon coupling strength and local condition of impurity centers. While the former two conditions can be controlled in the laboratory, finding a matrix that can greatly reduce the strength of the electron-phonon coupling and that will be able to provide unique local environment for the impurity centers is of eminent importance.

1.3 SHPOL'SKII MATRICES

In the foregoing section it has been pointed out already that a salient feature of the electronic or vibronic spectra of polyatomic organic molecules in solid solution is their high diffuseness. However, with the proper choice of solvent, quasiline luminescence spectra of these molecules in crystalline matrices can still be obtained at low temperature. In fact, to date most of the high resolution spectra of polyatomic organic molecules have been

acquired by this method. The strategy was originally put forward by É. V. Shpol'skii[36-38], who studied the high resolution spectra of a series of aromatic hydrocarbons dissolved in normal alkanes(paraffins). It turned out that quasiline spectra only resulted when a specific kind of aromatic hydrocarbon dissolved in a specific type of normal alkane. Consequently, this fact elucidated the mechanism of origin of these spectra named after their discoverer.

Normal alkanes, whose formulae are generally given by C_nH_{2n+2}, make good solvents for studies of molecular spectroscopy not only because of their chemical neutrality, but also because they are transparent even into the far UV region. Structurally, *n*-alkanes are zigzag chains with a period of 0.253nm(Fig.1.3).

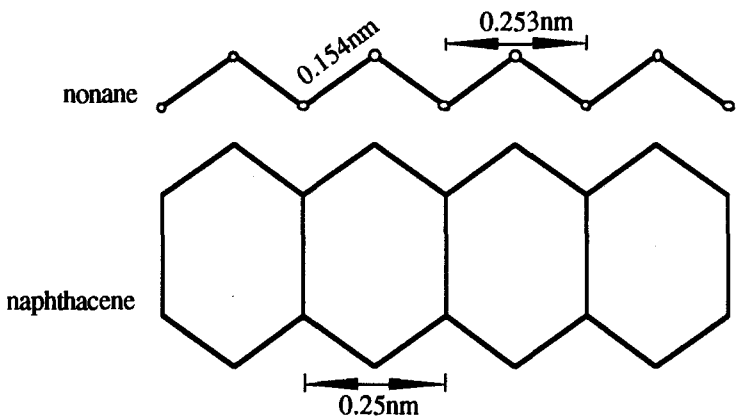

Figure 1.3 Zigzag structure of *n*-alkane and its dimensional and configurational relations with the impurity center when the best quasilinear spectra emerge. After[36].

The distance between neighboring carbon atoms is equal to the length of the aliphatic C-C bond in diamond structure(i.e. 0.154nm). Aromatic hydrocarbons, on the other hand, consist of condensed planar benzene rings, with a period of 0.25nm. From this, one can conjecture the reason as to why frozen *n*-alkane solvents yield spectral fine structure for

aromatic hydrocarbons: the period of the alkane chains agree with that of the aromatic hydrocarbons, so that they can be firmly imbedded in the surrounding alkane unit cells, with strictly defined orientation and without rotations*. However, if the length of the alkane chain does not agree with the long dimension of the aromatic hydrocarbon, the quasiline spectra will be diffuse and even smeared out, owing to the greater degree of freedom in the geometric arrangement of the molecules(for the case of chain length longer than molecular dimension) or collapse of the guest molecules(for short chain case). Early experiments[34] indeed showed that the host matrices of pentane, heptane and nonane were only effective for naphthalene, anthracene and naphthacene respectively, as guests and that the solvents could not be exchanged.

The above analysis provides us with a general guideline for the selection of suitable solvents, although in the case of the impurity molecules having more complex condensed arrangement of benzene rings, the conditions are no longer simple. Recently, Monte Carlo studies with an atom-atom potential model were made to understand the nature of the Shpol'skii matrix[39]. Such studies found that the porphyrin molecules were best interlocked in the Shpol'skii matrix formed by *n*-octane, which agreed well with the experiments[40,41]. The results illustrated therein were no more complicated than those simple pictures originally drawn by Shpol'skii[38]. Thus it suggests that simple graphical analysis, along with experimental searches, may be a reliable method for choosing the appropriate solvents in special cases.

1.4 ORGANIC SYSTEM STUDIED

---

* It was found later, however, that the orientation of the molecules in Shpol'skii matrices might not be unique. Several favorable positions, called sites, might simultaneously emerge.

The physically and chemically stable TBH_2Pc(mol. weight = 736), like its parent compound free base phthalocyanine(H_2Pc), is a derivative of porphyrins. These compounds are of importance due to their relevance in biological processes. For instance, it is well known that porphyrins, such as chlorophylls, play an important role in electron transfer processes in nature. On the other hand, the optical properties of these compounds in the visible and near UV regions are largely determined by the central porphyrin ring. Moreover, the TBH_2Pc has higher vibronic density of state and can much more easily dissolve in pure *n*-alkanes than H_2Pc do. Hence, investigating the relaxation processes in TBH_2Pc will contribute to the further understanding of these biologically active molecules. The dynamic electronic properties of phthalocyanines are of importance for their use as dyes, organic photoconductors and other applications.

To date there has not been any report on the structure of TBH_2Pc, although that of the H_2Pc has been revealed by X-ray[42] and neutron diffraction[43] analyses. In this thesis we only infer the structure of TBH_2Pc as that four tertiary butyl groups append on the outer benzene rings of the planar H_2Pc molecule, without causing any deformation and symmetry breaking of the phthalocyanine structure(Fig.1.4).

Of particular interest are the two protons attached to the aza-nitrogens in the kernel of the TBH_2Pc. As a result of the equilibrium positions of these two protons, two minima appear in the molecular potential scheme shown in Fig 1.5. However, these potential wells are not completely equivalent because the molecular structure has slightly deviated from D_{4h} to D_{2h} symmetry. Moreover, when the molecules are incorporated into a solid matrix, solvent effects may further enlarge this deviation. As a consequence, the TBH_2Pc possesses two tautomeric species, these two tautomers lead to the splittings in the absorption, emission and excitation spectra of TBH_2Pc.

It has been believed that the switching motion of the inner protons in porphyrin ceases at low temperatures but it can be induced by light[6,7,8]. By analogy, we expect

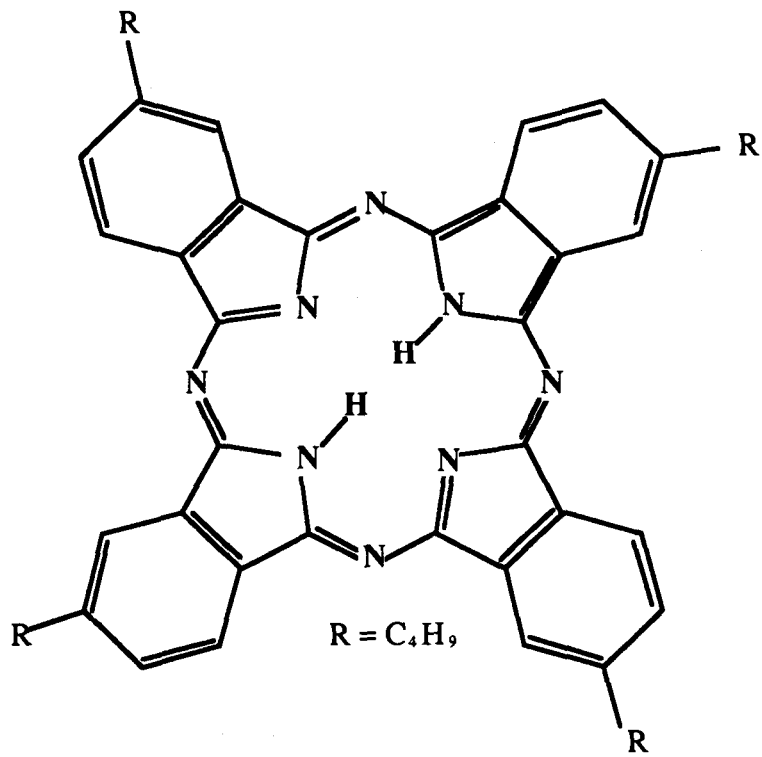

Figure 1.4 Spatial structure of TBH_2Pc by assuming that the addition of the tertiary butyl groups(R) does not cause distortion of the H_2Pc.

that such a photoinduced transformation between species will also occur in the TBH_2Pc molecule. In chapter 3 we present the results of a study of the phototransformation between the two tautomeric species of TBH_2Pc, in which we monitored the fluorescence intensity decay when the TBH_2Pc molecules were abruptly excited by a tunable dye laser. During the course our study, we found unexpectedly that the spontaneous transformation processes between the ground states of the two tautomers even occured without the presence of light(bottleneck effect). Thus, the investigation of the mechanism of these intrinsic dynamic processes of TBH_2Pc is the main theme of this thesis.

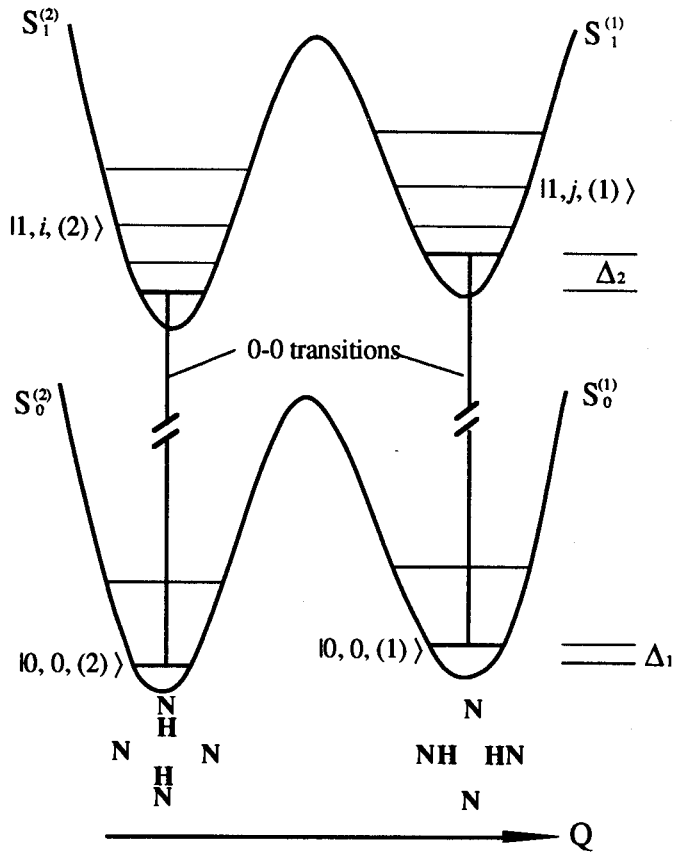

Figure 1.5 Schematic of energy levels of the two lowest singlet states of TBH2 Pc in Shpol'skii matrix. The molecular symmtery coordinate Q involving a rotation of the two inner protons. Spectral splitting is defined as $\Delta_2 - \Delta_1$ (Cf page 37 for the definitions of notations).

CHAPTER 2 EXPERIMENTAL APPARATUS AND TECHNIQUES

2. 1 EXPERIMENTAL APPARATUS

To design the experimental apparatus for the luminescence studies of molecules in frozen matrix, the following aspects should be considered: a narrow band tunable light source whose frequency range should be capable to cover the transition range of the molecule being studied and whose band width should be sufficiently narrow to carry out selected photoexcitation; a cryogenic environment for the sample, light dispersion equipment and signal collecting, processing, recording devices. This leads to our experimental setup that is shown schematically in figure 2.1. It can be divided into three related sections: excitation section, cryogenic section and data acquisition section. We shall describe these sections separately.

2. 1. 1. Excitation of Samples

This section consisted of a 4-watt Coherent 52G argon ion laser, a Coherent CR599 dye laser, a homemade stepmotor and other peripheral devices. All visible lines(but mainly 514.5nm and 488.0nm) from the ion laser provided continuous pumping for the dye laser. When fully pumped, the dye laser was able to produce 120-150mW monochromatic output. The dye was chosen to be DCM(4-(Dicyanomethylene)-2-methyl-6-(p-dimethylaminostyryl)-4H-pyran) dissolved at a concentration of 1.5×10^{-3}M in benzyl alcohol and ethylene glycol 1:5 mixture, its high pump efficiency and its wide tuning range from 13330cm^{-1} to 16390cm^{-1} are suitable for the excitation of the TBH_2Pc molecules from the ground states to the first excited electronic and vibronic states. A two-plate birefringent

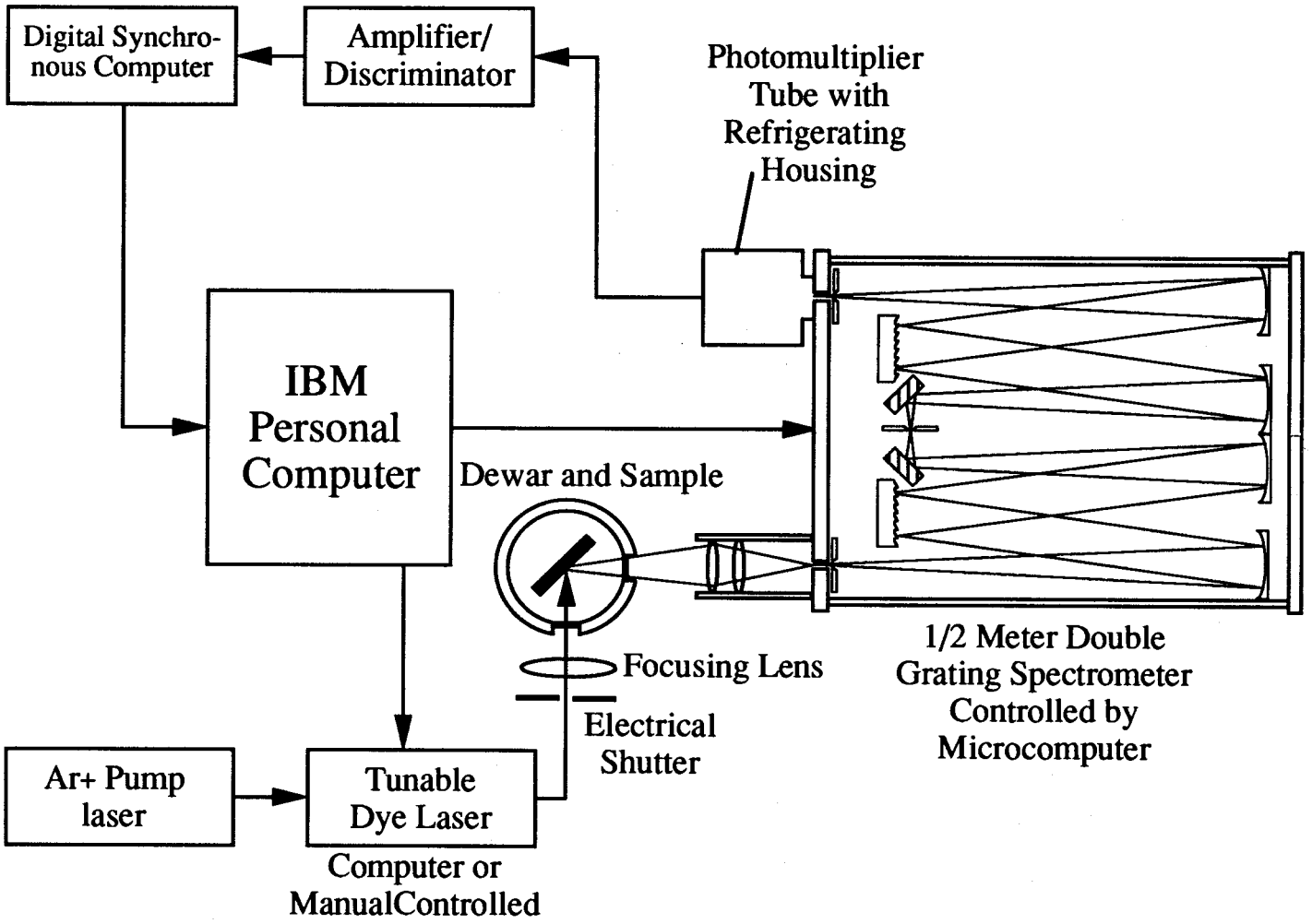

Fig. 2.1 Schematic illustration of the experimental setup

filter at the Brewster angle with respect to the horizontal was inserted into the folding cavity of the CR599; it played the role of wavelength selector. Turning the graduated thumbscrew on the filter's housing would change the angle between the two birefringent axes, and the output with $2cm^{-1}$ FWHM(full width of half maximum) of its Guassian profile and desired wavelength was selected. The thumbscrew could be controlled manually or through the stepmotor driven by the microcomputer. The correspondence of wavelengths and scale readings on the thumbscrew must be calibrated as frequently as possible with the aid of the spectrometer.

2. 1. 2. Cryogenics

Experiments at the boiling temperatures of nitrogen and helium were performed separately from those at other temperatures, using a multilayer glass dewar shown in figure 2.2. To achieve the maximum thermal insulation, the two vacuum layers of the dewar were pumped to 2×10^{-5} torr with a diffusion pump. The sample, located at the center of the inner chamber was immersed in the liquid helium or nitrogen. Except for two one-cm-wide stripes at twelve and three o'clock positions on the dewar wall providing the entrance and exit of the light, the entire dewar was silvered. Liquid N_2 was filled into the middle layer to precool the inner chamber, as this would advoid excessive vaporization of liquid He during transfer. Temperatures below 4.2K could also be obtained by reducing the helium vapor pressure using a Stokes pump.

A commercial stainless steel dewar was used for the temperature variation experiments(figure 2.3). Injecting cold gas helium to the sample can vary its temperature above 4.2K. Originally, an ideal temperature control unit should have included an automatic helium valve controlled by the feedback signal from the temperature sensor and a heater near the sample. However, since the requirement on the accuracy of temperature in our experi-

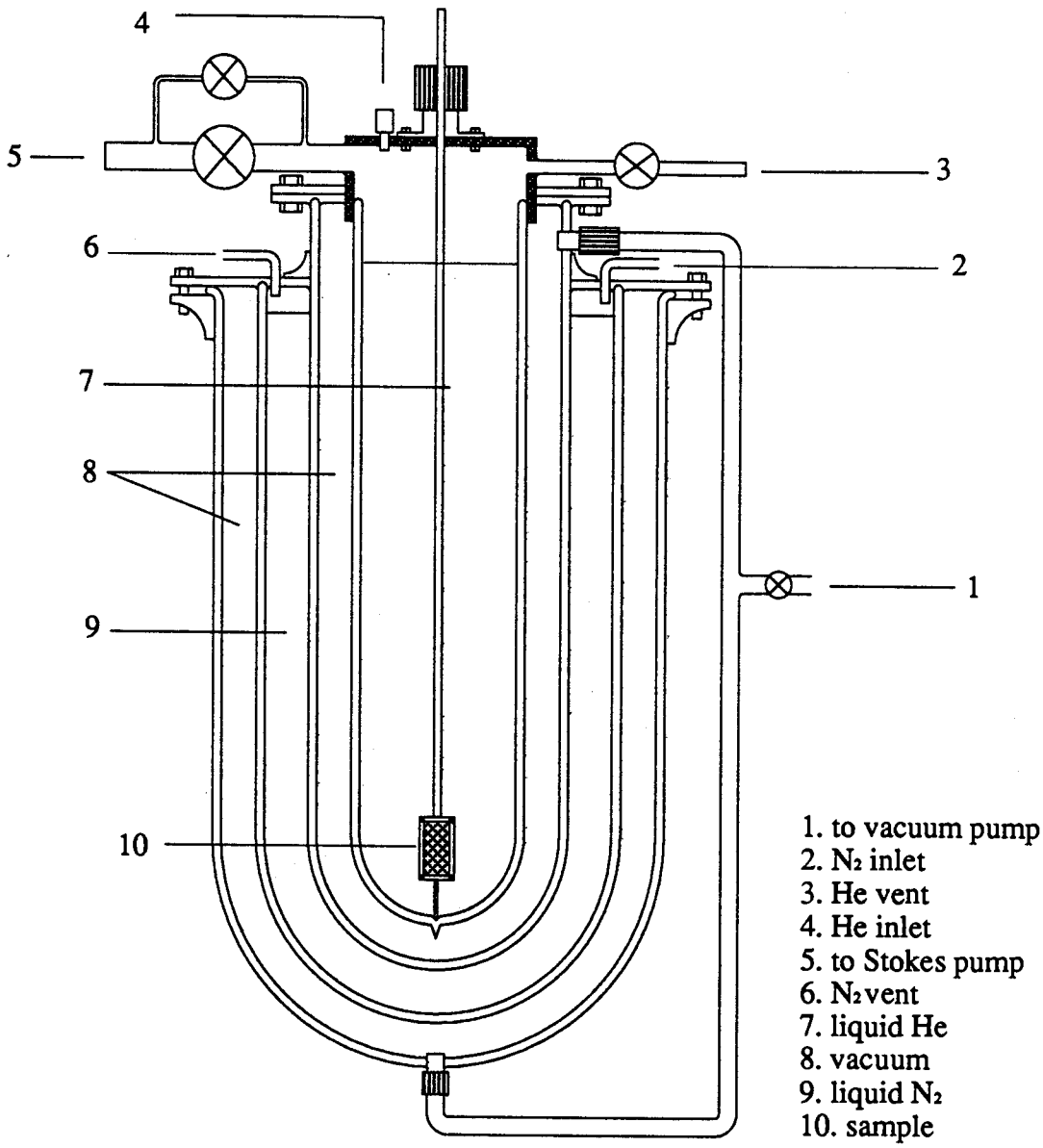

Fig. 2.2 Sectional drawing of the glass dewar used in the experiments at 4.2K and 77.3K

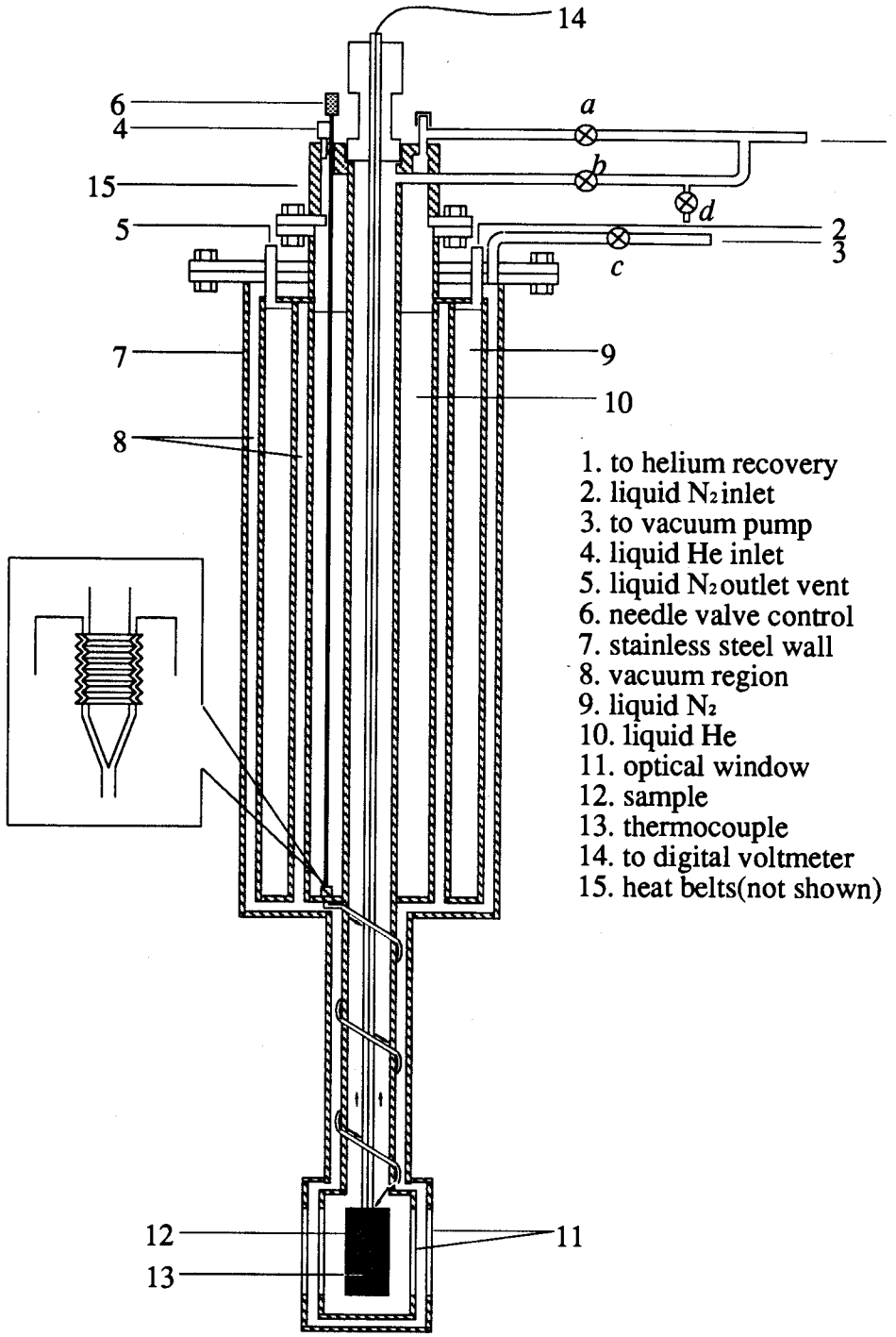

Fig. 2.3 Metal dewar for the temperature variation experiments
The inset shows the needle valve magnified

ment was not critical, the apparatus could be simplified by building a threaded needle valve at the bottom of the helium chamber, such that the helium flow was being able to transferred through the spiral capillary tube to the sample chamber. A long steel rod extended this needle valve to the exterior of the dewar, so that the valve could be adjusted manually. Furthermore, closing or half closing the helium vent valve *a* would increase the vapor pressure in the helium chamber, thus increasing the flow rate in the case when insufficient helium flowed to the sample chamber, despite of the total opening of the needle valve. The vacuum separating the chambers was again pumped to 2×10^{-5} torr and liquid nitrogen was used as thermal buffer. However, due to the inherent thermal conductivity of the metal dewar, it was absolutely necessary to twine heat belts on the upper part of the helium chamber that extends outside the dewar. Such heat source balanced the rapid cooling caused by the liquid He, especially when it was being transferred, thus minimizing the contraction of the dewar and softening the O-ring seals, preventing vacuum leakage of the dewar. Fused silica optical windows on the sample chamber were also sealed by indium wires in order to withstand 10^{-5} torr of vacuum.

Temperature measurements of the sample were carried out by a type T(copper/copper-nickle) thermocouple whose reference junctions were being placed in 0°C ice water and whose detection junction was immersed directly into the sample to ensure the optimal thermal contact. The voltage V vs temperature T characteristic curve is shown in fig.2.4. Although such a thermocouple loses most of its sensitivity at very low temperature(e.g.~1.2μV/K at 5-10K), yet a DANA 5000 digital voltmeter with an accuracy of 1μV still provided an accuracy of ±1K or better in our experimental temperature range and made this simple, inexpensive thermometer feasible. Owing to the fact that the thermocouple used in this experiment might not follow exactly the standard T-V curve, it had been calibrated against the NBS standard[44] by applying the following equation:

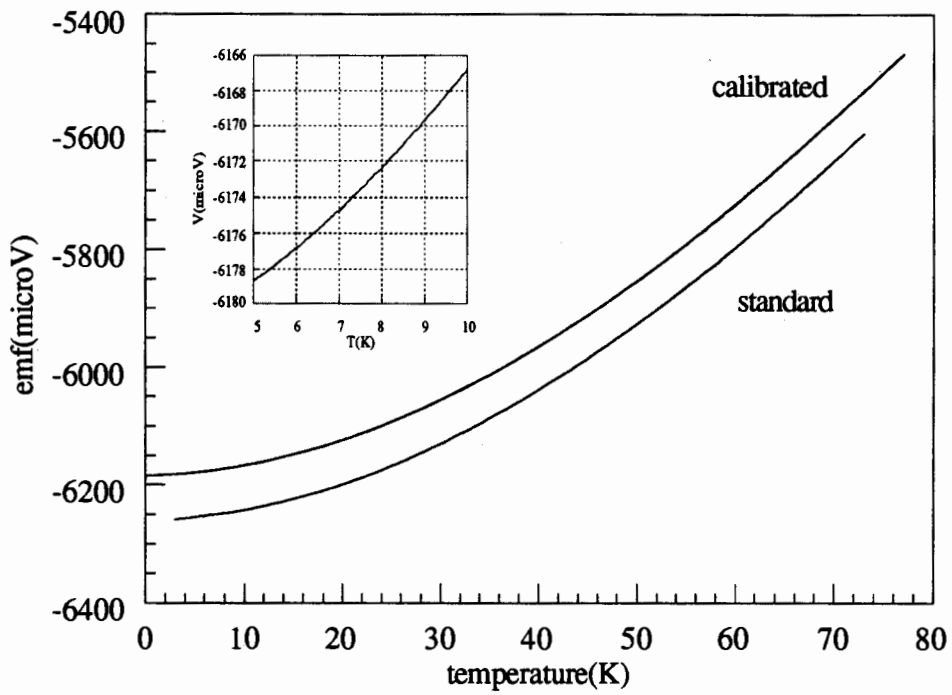

Fig. 2.4 T-V Characteristic of type T thermocouple with ice/water reference
The inset is the magnified low temperature region showing the
sensitivity of the thermocouple. Data after [44].

$$\Delta_n = \frac{\Delta_2 - \Delta_1}{T_2 - T_1} \times (T_n - T_1) + \Delta_1 \qquad (2.1)$$

where T_1 is the first calibration temperature

T_2 is the second calibration temperature

T_n is any temperature between T_1 and T_2

Δ_1, Δ_2 and Δ_n are voltage deviations from the NBS standard at T_1, T_2 and T_n respectively.

The above interpolation is based on the assumption that the deviation of voltage from the standard is a linear function of the temperature between the two calibration points. The T_1 and T_2 were chosen to be 4.2K and 77.0K, which were the boiling temperatures of helium and nitrogen under the atmospheric pressure at Burnaby Mountain; and the Δ_1 and Δ_2 were 88 and 86 μV respectively. Once Δ_n was obtained, a new calibration curve could be formed, and the voltage readings could be converted into temperatures.

2. 1. 3. Data Acquisition and Processing

While an ordinary convex lens focused the laser light onto the sample, a f = 45 - 135mm, 1:3.5 photographic lens focused the optical signals emitted by the sample onto the entrance slit of a SPEX 1301 0.5meter double grating spectrometer. The spectrometer has a 5-digit odometer-like wavelength display that permitted a reading accuracy to 0.1cm^{-1}. After the signals were dispersed by two 1200-groove/mm gratings, only light with a wavelength displayed on the counter was able to pass the ganged intermediate and exit slits, arriving at a ITT FW130 photomultiplier tube for photon counting.

However, there always existed discrepancies between the true and displayed wavelengths; such discrepancies were caused by the backlash of the threads in the grating control unit, but they could be calibrated against the following standard neon lines[45] with linear interpolation.

Table 2.1 Deviations of spectrometer wavenumber display in different spectroscopic region

standard wavenumber(cm^{-1})	deviation(displayed - standard)(cm^{-1})
14236.8	1.7
14431.1	1.8
14887.5	1.6
14973.9	1.6
15032.9	1.6
15307.2	1.5
15369.2	1.5
15516.6	1.5
15572.2	1.5
15619.5	1.5
15666.6	1.5
15743.4	1.4
15786.7	1.4
15802.4	1.4

The FW-130 PM tube with a S20 response was installed into a -20°C refrigerating housing to reduce the thermal noise. The cathode voltage was set above to 2100V, a high

setting that compensated the age of the tube. The calibration on the frequency and intensity responses seemed unnecessary for the reasons that will become clear later.

The photomultiplier output fed into a model 1120 amplifier/discriminator(A/D), a SSR model 1110 digital synchronous photon counting computer(DSC) constituted the photon counting signal acquisition section. Due to the necessarily low level signals involved and the wide bandwidth of the system that permitted high speed counting, the 1120 A/D was highly susceptible to the interference of radio signals from external sources. Therefore, the A/D and its connection to the PM tube anode were heavily shielded.

DUAL mode was one of the diverse modes of the 1110 DSC, it was selected to accumulate the number of counts sent from the D/A within certain preset time interval(preset time per channel). The 3-digit switch on the front panel determines the time duration of 1 channel N, which could vary from 1μs to 999s.

Whenever a counter is used, its dead time τ must be considered. Such τ, as we shall see later, has a direct impact on the accuracy of photon counting as it may enlarge the actual time scale of any time resolved process by a considerable factor. It is inherent though because the DSC must distinguish the countings of two channels. Ideally, τ should be several orders of magnitude shorter than N, the acquisition time(Fig. 2.5). For the 1110 DSC, however, such τ was comparable to N. In fact, the scanning time of the DSC was always found to be longer than the product of the preset time per channel N and the number of channels. Although no information for the τ was provided, it could still be found by the following simple method: select a preset time per channel N, using a stopwatch to measure a certain period of time t during which a weak laser beam is incident on the slit of the spectrometer; then the number of channels receiving the light should theo-

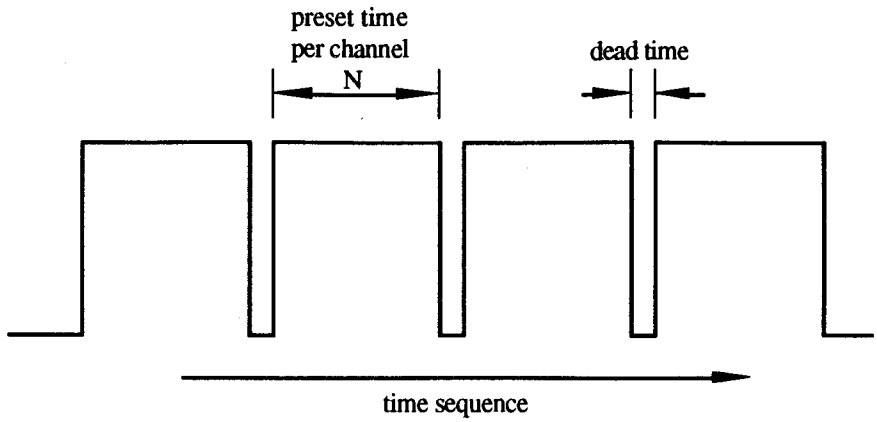

Fig. 2.5 Time sequence of the photon countings of the SSR 1110 DSC

retically be t/N. However, we can also obtain from the recorder the actual number of channels n that received the light, thus the dead time

$$\tau = \frac{t - nN}{n}. \tag{2.2}$$

As indicated in table 2.2, the dead times were found to be 3.3 milliseconds for the preset N=0.01s and 0.05s. These two settings were used in the later experiments.

Table 2.2 Calibration results for two preset N's

N(sec./chan.)	t(sec.)	n(chan.)	τ(msec.)	ave. τ(ms)
0.01	15±0.5	1128	3.3±0.4	
0.01	15±0.5	1124	3.3±0.4	3.3±0.2
0.01	15±0.5	1128	3.3±0.4	
0.05	50±0.5	938	3.3±0.5	
0.05	50±0.5	939	3.3±0.5	3.3±0.3
0.05	50±0.5	939	3.3±0.5	

An IBM personal computer played a role of central control of data acquisition and display in this experiment. On one hand it manipulated the slew of the spectrometer and on the other it recorded, displayed and stored data from the DSC, by executing a software program *MONO* (developed and made available by Dr. P. Milford). The main functions of this software used in the experiment were: 1. it slewed the gratings to any wavelength position that the experimenter desired(in the future, "move the spectrometer to certain position" will imply that the gratings of the spectrometer are moved to certain wavelength position); 2. it scanned the gratings within a certain wavelength range. The initial and final wavelength positions, as well as the change in wavelength per step, could be arbitrarily set. But the scanning speed, in terms of the time duration per step, was determined by the 3-digit switch on the DSC that has been mentioned before(this is exactly the preset *N*); 3. it collected data from the DSC while keeping the gratings in fixed position. The collecting speed was again determined by the preset *N* of the DSC. Finally, the recorded experimental data were processed for future analysis and graph drawings by softwares which were commercially available(Borland's *Quattro Pro* and *KaleidaGraph* of the Abelbeck Company).

2. 2. EXPERIMENTAL TECHNIQUES

2. 2. 1 Sample Preparation

The commercially unavailable TBH_2Pc was provided by Prof. D. Haarer of the Universität Bayreuth. This blue powder was weighed and dissolved in Aldrich 99+% anhydrous hexadecane to make up a solution with a concentration of $(1.00\pm0.05)\times10^{-4}$M. High concentration was avoided since it might cause two possible unfavorable effects: the quenching of fluorescence in high concentration and the concentration transformation sug-

gested by Förster and Kasper[46]. It has been pointed out[36] that oxygen would also quench the fluorescence intensity by a considerable amount, so that air must be carefully evacuated from the 1cm×2cm×1mm glass cell containing the sample solution. Then the sample cell can be fixed onto the copper cage at the end of the sample rod, which is in turn inserted into the dewar's inner chamber.

It is a known fact[47] that rapid cooling of the sample may prevent crystallization and creat an amorphous solid matrix, thus broadening the inhomogeneous linewidth. Therefore, in our experiments, the sample was first placed into the inner chamber before any transfer of the coolant, then a slow cooling process(approx. 4K/min.) was carried out by the temperature gradient generated from the liquid N_2 in the buffer layer. Liquid He was only transferred after the sample was completely crystallized.

2. 2. 2 Searching the Energy Levels of the TBH_2Pc

Previous studies of the TBH_2Pc molecules[48,49] had given us information about the energy separation between its ground and first excited singlet states. To obtain the exact energy levels of TBH_2Pc, the sample was irradiated with intense laser light. The 0-0 transition wavelength regions suggested by the above references were then scanned with the spectrometer. As this procedure was repeated using various excitation wavelengths, it was most likely for us to observe a trace of 0-0 transition, even though the laser might not be resonant with the molecule's energy level. The spectrometer was then moved to the approximate 0-0 transition position and the laser finely tuned to the wavelength that produced the strongest fluorescence intensity. Then the aforesaid region was scanned again. In this way, the exact wavelength positions of the 0-0 transition could be approached by successive repeats of the procedure.

The complex vibronic structure of the first singlet excited state could be obtained by fluorescence-excitation spectroscopy. The excitation wavelength was continuously varied while at the same time constantly monitoring the fluorescence signals at the 0-0 positions(since two tautomers existed in the TBH2Pc, two set of fluorescence-excitation spectra were obtained). This was accomplished by activating the stepmotor that was connected to the laser birefringent filter's thumbscrew. However, spectra with the best resolution could only be obtained when several parameters of the instruments were well coordinated. They were: the slitwidth of the spectrometer, the preset time per channel *N* of the DSC, and the rotation speed of the stepmotor.

Because of the limited intensity of the fluorescence signals, wide slitwidth and long *N* seemed favorable for obtaining a good spectrum. However, one had to consider slitwidth in terms of spectral bandpass. Under the conditions of fixed grating constant, fixed wavelength and spectral order, bandpass was a function of the slitwidth. In our wavelength regions of interest, 100μm and 250μm of slitwidths correspond to 1.0cm^{-1} and 5.0cm^{-1} bandpasses respectively. Also, a shorter a data collection time per channel would mean higher resolution of the spectra. On the other hand, one revolution of the thumbscrew changed the laser wavelength by approximately 140cm^{-1}, thus appropriate motor speed would quicken the experimental procedure without losing spectral resolution.

Having compromised the intensity and resolution, the slitwidth was set to be 100μm(to allow 1.0cm^{-1} bandpass) and *N* =0.5second/channel. That is to say, the rate of the wavelength change should not exceed 0.5cm^{-1} per 0.5 second, which was in turn equivalent to the motor speed of 0.4rpm, in order to retain ±1cm^{-1} resolution.

Up to this point we had only a picture of fluorescence intensity vs time. To convert the time scale to that of the wavelength, we purposely closed and reopened the shutter as

quickly as possible at the moment of that the thumbscrew scale passed a certain point, so that "dark marks" were stamped on the picture. Together with the wavelength-thumbscrew scale calibration table, these "dark marks" provided references for the future time-wavelength conversion. Taking the uncertainty introduced by linear interpolation into account, the wavelength accuracy of the fluorescence-excitation spectra was estimated to be within $\pm 2cm^{-1}$.

2. 2. 3. Phototransformations of the TBH_2Pc Molecules

As has been indicated in chapter 1, phototransformation of TBH2Pc molecules in frozen matrix manifests itself by exponential fluorescence intensity reduction effects after sudden step excitation of the sample with laser light. To observe this exponential effect, we indentified one of the vibronic levels of the molecule according to the fluorescence-excitation spectra and finely tuned the excitation wavelength so that it was resonant with this level. After excitation at this wavelength had led to a steady state, a dark pause(in the order of few to tens of seconds) was given to the sample and the fluorescence intensity as a function of time was recorded upon renewed step excitation. The slitwidth was not of importance in this type of experiment and it was set to 200μm. However, the setting of N must be chosen more carefully. That is, N must be short enough to resolve the transformation processes(whose characteristic times are typically tens of millisecond). But because of the problem of "short-N-low-counts" an optimal compromise must be found. As table 2.3 indicates, low photon counts inevitably results in high counting error.

In this experiment, N = 0.05sec/channel yielded 10^2 to 1×10^3 counts per channel. Because of this error, data were acquired statistically: 10 trials for each parameter combination. As for the temperature dependent experiments, the above procedures were followed, and the uncertainty of the temperature was controlled within ±1K.

Table 2.3 Percent Error of Photon Counts of the SSR1110 DSC*
(95% Confidence Level)

Counts per Channel	Percentage Count Error	Counts Per Channel	Percentage Count Error
100	20.0	2,000	4.5
200	14.2	5,000	2.2
300	11.6	10,000	2.0
500	8.9	50,000	0.89
1,000	6.3	100,000	0.63

* After SSR 1110 DSC technical manual, Princeton Applied Science

CHAPTER 3 RESULTS AND DISCUSSION

We start this chapter by considering how TBH_2Pc may be embedded in solid matrices. We thereby arrive at the criterion for the appropriate solvent(s) for TBH_2Pc that are most likely to give good Shpol'skii spectra. In the same section, fluorescence and excitation spectra of TBH_2Pc are presented. These spectra not only reveal the electronic and vibrational structures of the TBH_2Pc but also provide confirmation of the validity of the aforesaid criterion. Section 3.2 will discuss the mechanism and pathways of the photoinduced relaxation processes between excited states. The spontaneous relaxation process in ground states, along with a theoretical model, will be discussed in section 3.3.

3.1 HIGH RESOLUTION SPECTRA OF TBH_2Pc AND THE SHPOL'SKII EFFECT

3.1.1 Geometrical Analyses of Molecules

In section 1.3, we have stated that highly resolved luminescence spectra of polyatomic molecules can be acquired, given that at low temperature the spatial dimension of crystalline solvent cells are correlated with that of the guest molecules. Such spectra are referred to as Shpol'skii spectra. A good Shpol'skii spectrum should possess small inhomogeneous linewidth and a weak the guest-host interaction so that the guest molecule retains its level characteristics with minimal perturbation from the host. For our TBH_2Pc molecules we expected *n*-alkanes would be the appropriate solvents, because their absorption bands are in the region above $65000cm^{-1}$[50], remote from the absorption regions of many organic aromatic molecules; their zigzag structures appear to be compatible

with benzene ring structures, also the length of the hydrocarbon chain can be changed almost arbitrarily to accommodate the guest molecules. More importantly, TBH_2Pc differs from the H_2Pc in that it can be dissolved up to 10^{-4}M into pure *n*-alkanes(while for latter mixed solvent of α-chloronaphthalene and *n*-alkanes must be used in order to achieve the concentration necessary for the detection of the luminescence signals[51]). Appropriate alkanes for TBH_2Pc can be found empirically, as has been reported in [52], but such attempts are rather haphazard. Some of the *n*-alkanes with an odd number of carbon atoms(e.g. undecane, tridecane, pentadecane) were not tried in this study[52]. As a result, certain potential candidates for forming good Shpol'skii matrices might have been ignored. In this study, we employed a semi-quantitative spatial analysis of the TBH_2Pc molecule and the crystalline *n*-alkane. This analysis is not as rigorous as a Monte Carlo analysis[39], yet it still provides us a general guideline of selecting the most appropriate matrix and it also enables us to graphically visualize how impurities may be incorporated into the solid matrix.

The probable structure and dimension of the *n*-alkane chain has been illustrated in chapter 1(Fig.1.3). X-ray diffraction study[53] shows that the unit cells of *all* crystalized *n*-alkanes are orthorhombic, and that they have the same dimension in the directions of the *a* and *b* axes(Fig. 3.1), namely a=0.745nm, b=0.497nm. There are four alkane chains that coincide with the four edges of the orthorhombic cube, hence the height *c* of the cube increases linearly with the number *n* of carbon atoms in the *n*-alkane molecule. The short axes of these four chains are oriented in the (110) direction of the cell. There is also a fifth chain, whose short axis is in (-110) direction, located at the center of the cell.

We now proceed to analyze the structure of TBH_2Pc molecule by assuming that the distortion of H_2Pc backbone introduced by the addition of the four tertiary butyl radicals is insignificant. This assumption allows us to attach the tertairy butyl radicals geometrically

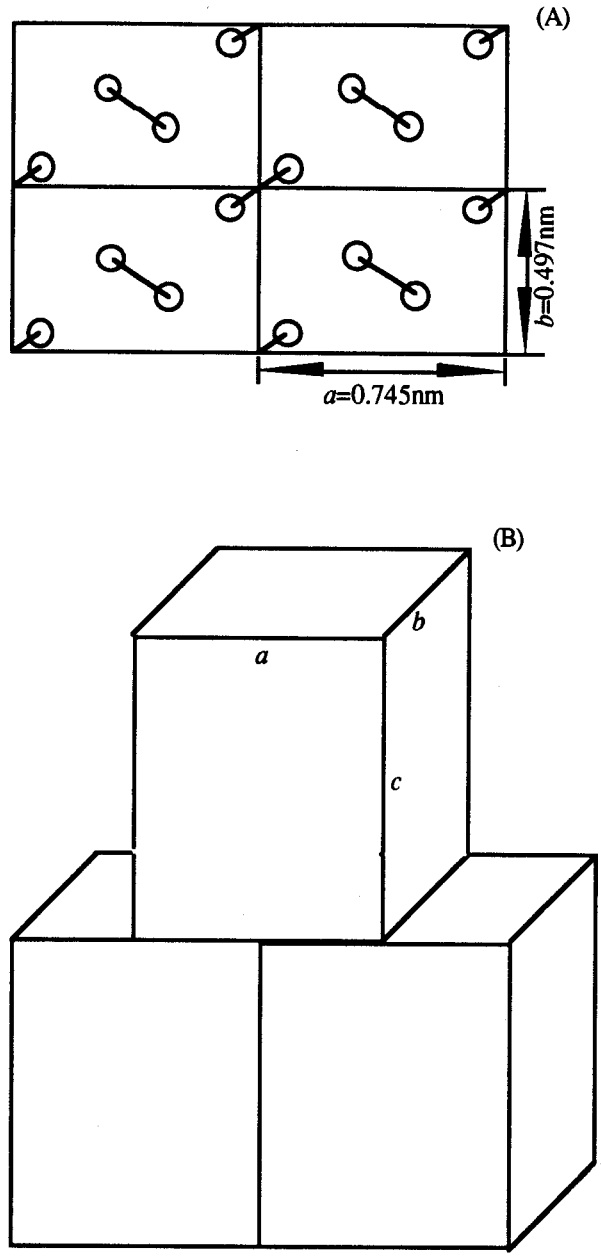

Figure 3.1 Arrangements of crystalized alkane unit cells. (A) view from (001) direction, all alkanes have the same a and b. (B) view from (111) direction, unit cell are staggered, and c depends on the length of alkane chains

to the vertices of the outer benzene rings. The positions of the periphery atoms in the H_2Pc backbone are, with respect to the cartesian coordinates originating at the symmetry center of the molecule(fig. 3.2), given in table 3.1.

Table 3.1 Positions of Selected Atoms in H_2Pc and TBH_2Pc molecule(Cf. fig.3.2)

Atoms	Positions x(nm)	Positions y(nm)
1, 4, 1', 4'*	±0.420	±0.507
2, 5, 2', 5' *	±0.517	±0.408
3, 6, 3', 6' *	±0.477	±0.275
13, 13', 14, 14' *†	±0.132	±0.138
7, 7' **	±0.505	±0.803
8, 8' **	±0.345	±0.642
9, 9' **	±0.554	±0.582
10, 10 **	±0.815	±0.485
11, 11' **	±0.704	±0.297
12, 12' **	±0.628	±0.595

We also take the C-C bond lengths in the C_4H_9 groups to be 0.154nm, which identical to those in alkanes. Then the dimension of the TBH_2Pc molecule are estimated to be 1.60nm×1.55nm. Taking the radii of the carbon atoms (0.077nm) into account, these numbers are correlated to twice the diagonal length(i.e. 1.79nm) in the (011) direction of the *n*-alkane unit cell. Such correlation strongly suggests that one possible position of the

* Data for H_2Pc, after Robertson[42].
** Calculated values for TBH_2Pc.
† Will be used in section 3.2.2.
The "±" signs indicating the quadrant in which the atom situated.

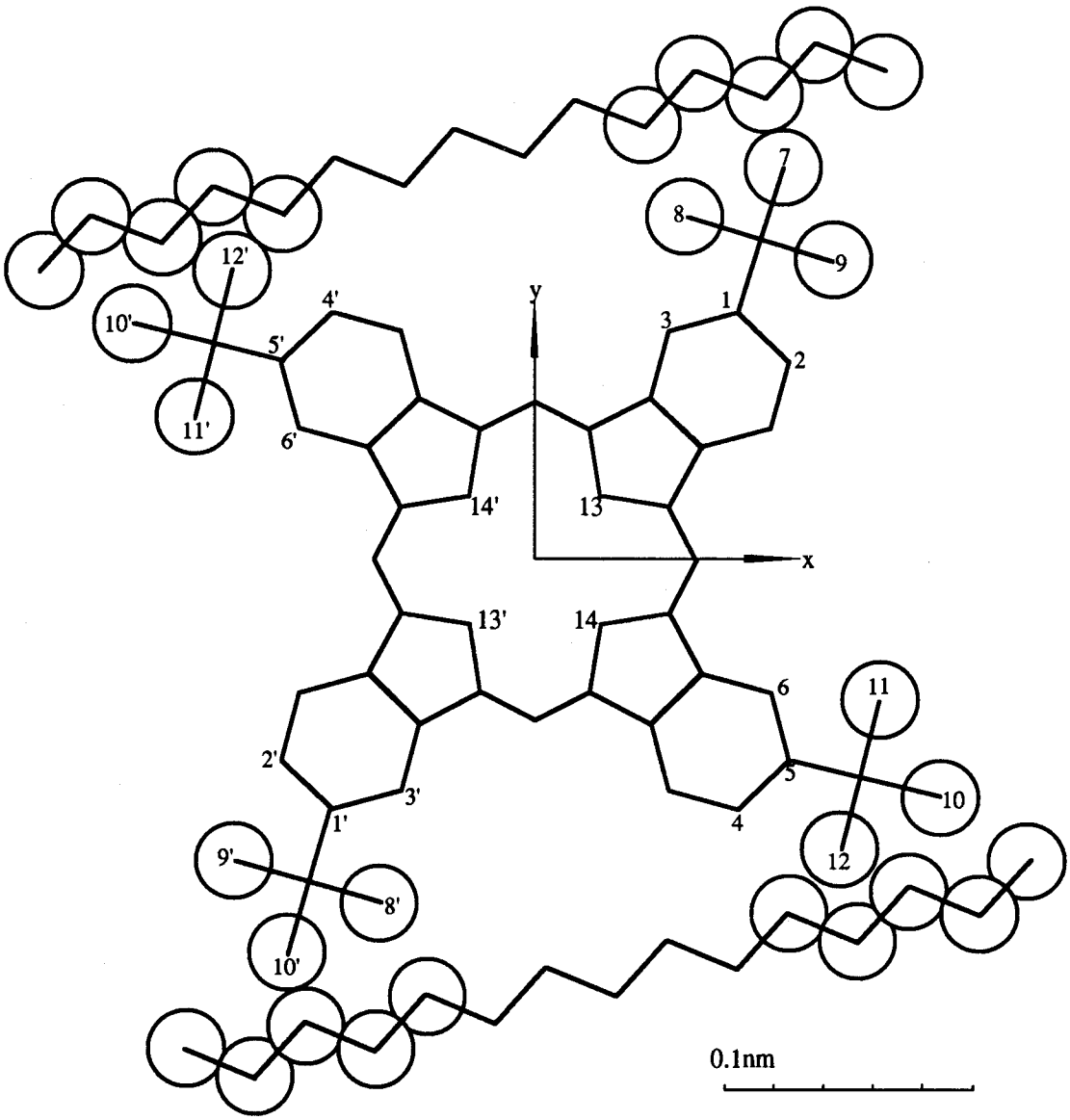

Figure 3.2 One possible position of TBH_2Pc molecule in crystalized normal alkane base on ball-and-stick model. The molecular plane lies in the (110) plane of the alkane unit cell. And the graphic shows that pentadecane may be the most appropriate solvent for this particular kind of molecule. All positions and interatomic distances are strictly in proportion.

TBH_2Pc molecule embedded in the crystalized alkane may be that the molecular plane of the planar TBH_2Pc lies in the (110) plane of the alkane unit cell, replacing three alkane chains. If so, we can also deduce from the graph that the chain length for forming the best confinement should be about 1.75nm(again radii of carbon atoms must be considered), which corresponds to the chain length of one in tetradecane, pentadecane or hexadecane. Any alkane whose chain length is considerably shorter or longer than this may cause collapse of the ordered structure into an amorphous on or introduce larger degree of freedom for possible microstructures surrounding the TBH_2Pc molecule. This will broaden or eliminate Shpol'skii spectra.

3.1.2. Fluorescence and Excitation Spectra of TBH_2Pc

To verify the prediction made in the previous section, we dissolved the TBH_2Pc into tetradecane, pentadecane and hexadecane respectively, all with concentrations of 1 $\times 10^{-4}$M. Then these solutions were slowly cooled down to liquid helium temperature. The estimated energy difference between the first excited state S_1 and ground state S_0(0-0 separation) of TBH_2Pc was given by Rebane *et al* as 14420cm^{-1}[48]. Thus the samples were excited a few hundreds wavenumbers above this region* , and fluorescence signals were recorded in that vicinity. Figures 3.3(a)-(c) illustrate the fluorescence spectra of TBH_2Pc in the three solvents. They are typical Shpol'skii spectra, with quasilinear lines superimposed on a broad background that spread over several hundreds of wavenumbers. Some characteristics of these spectra are summarized in table 3.2. Electron-phonon interaction between the guests and hosts and the possibility of a mixture of crystalline and amorphous regions in the sample are responsible for the inhomogeneous backgrounds in figure 3.3. The side bands extend to low energy regions, indicating that electronic transitions are ac-

* The excitation wavelengths are not arbitary, they must be resonant with certain vibrational levels, which can be found from excitation spectra.

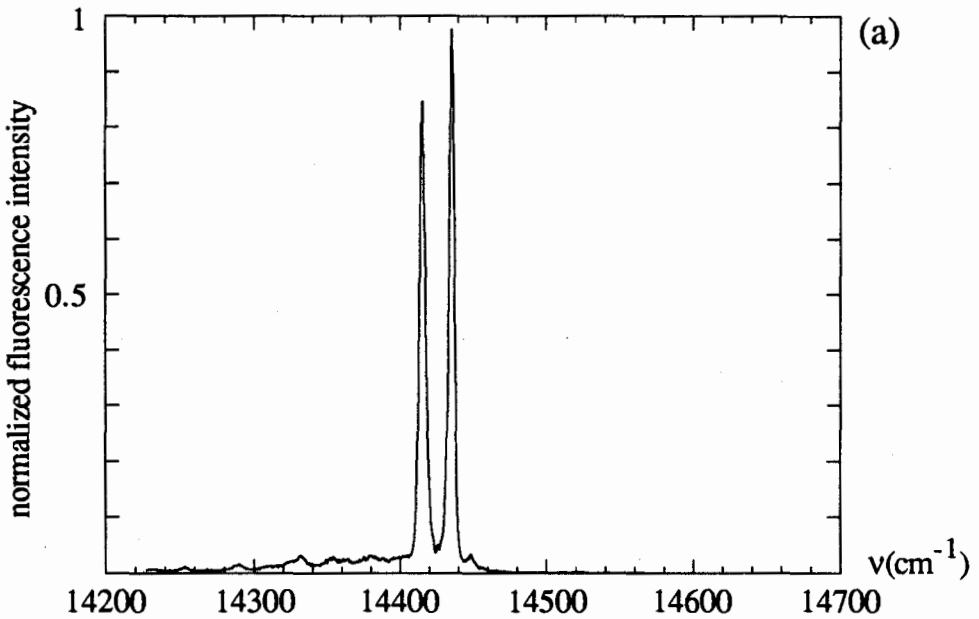

Figure 3.3. 0-0 fluorescence of TBH_2Pc in (a) hexadecane, (b,next page) pentadecane, and (c) tetradecane matrices. The doublets are the results of the molecule's intrinsic asymmetry and distortions caused by matrices. The spectral splittings are (a)21, (b)15, (c)12cm^{-1}.

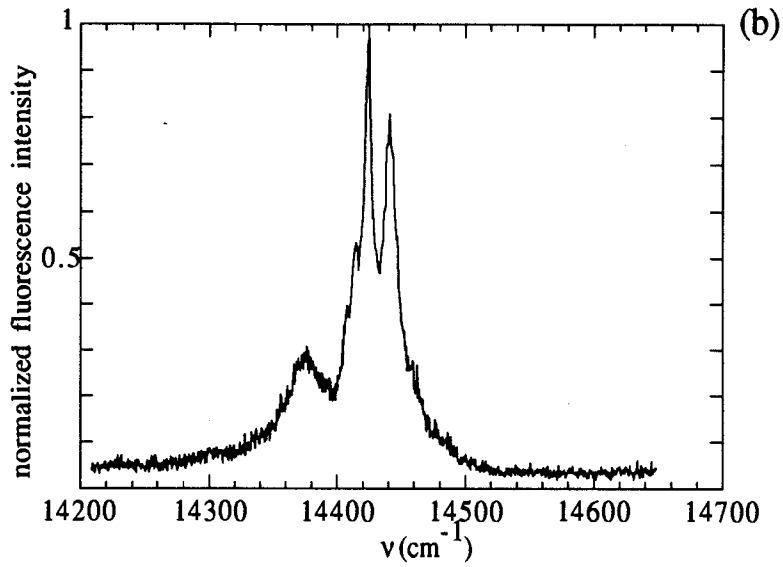

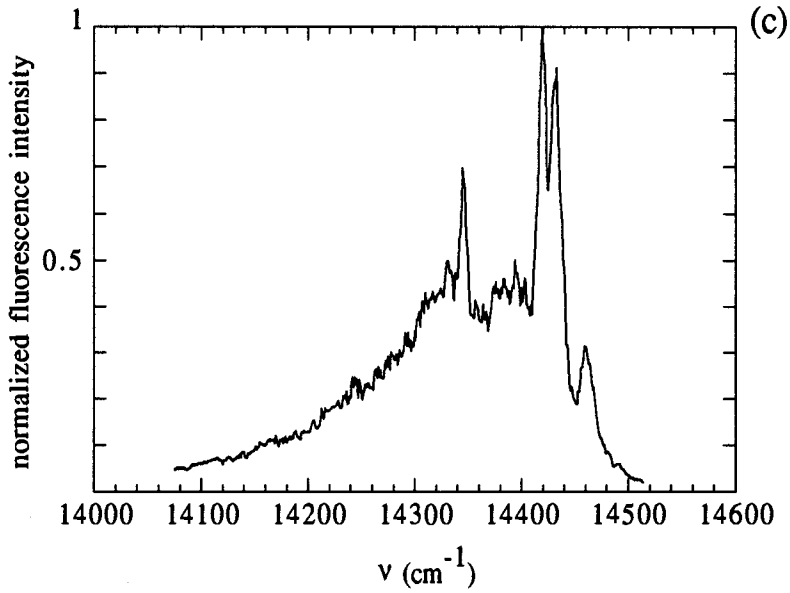

Figure 3.3 (continue)

companied by the creation of phonons. In the spectra of TBH_2Pc in hexadecane the electron-phonon interaction is minimized, resulting in a Debye-Waller factor very close to unity. All fluorescence linewidths are $<15cm^{-1}$, but they are still far from homogeneous(usually of the order of $10^{-3}cm^{-1}$). Wider Shpol'skii linewidths result either from the guest being only loosely confined and retaining the freedom to be randomly oriented the surrounding crystalline structure or from the guest being too big to be comfortable incorporated into a crystalline structure, with the resulting stresses collapsing the ordered structure and leading to an amorphous structure. From this we conclude that hexadecane confines TBH_2Pc molecules more firmly than the other two solvents do, because the linewidth of this spectrum is less than that from the others and its background is negligible.

Table 3.2 General Characteristics of Fluorescence Spectra of TBH_2Pc in *n*-alkanes

n-alkane	Debye-Waller factors	FWHM (cm^{-1})	Positions of two maj. peaks(cm^{-1})	Splittings (cm^{-1})
tetradecane	~0.72	10 ~ 12	14420±1 14432±1	12
pentadecane	~0.83	13 ~ 14	14425±1 14440±1	15
hexadecane	~0.95	5 ~ 6	14415±1 14436±1	21

Spectral splitting is another indication of the tightness of guest molecules being confined in solid matrices. The fluorescence doublets in figure 3.3(a)-(c) are unequivocally identified as the 0-0 transitions of the TBH_2Pc by their intensities, and the nature of the doublets originates from the asymmetrical molecular potential wells(Cf fig.1.5, page 10) caused by the two chemically non-equivalent tautomers(Following the convention[58], we use superscripts to specify different tautomeric species. Superscript (1) represents that

with higher 0-0 transition, and (2) represents the other. So the excited and ground states now become $S_1^{(1)}$, $S_1^{(2)}$, $S_0^{(1)}$, $S_0^{(2)}$ etc.). Early experiments showed that similar 0-0 fluorescence splittings of free base chlorin could reach 1600cm^{-1}[54,55], two orders larger than that of the free base porphyrin(<100cm^{-1})[56,57]. Chlorin only differs from porphyrin in structure by reducing a double bond in one of the pyrode rings of the porphyrin so that its degree of symmetry is less than that of porphyrin. We conclude that molecular symmetry greatly influences the spectral splitting. If TBH_2Pc is held more tightly by hexadecane than by the others, it will be subjected to stronger external forces that cause larger molecular distortion, so the splittings will be larger. This is what was observed and as shown in figure 3.3(a) and table 3.2.

We now briefly discuss the excitation spectra of TBH_2Pc in hexadecane (figure 3.4a)and pentadecane(figure 3.4b). Excitation spectra are acquired by continuously changing the excitation energy while monitoring the 0-0 fluorescence intensity. Once the excitation is resonant with a vibrational level, this level will rapidly decay to the vibrationless level of the first excited states, from which the molecule fluoresces to ground levels. Because there are always two tautomeric species for TBH_2Pc molecule, we expected to obtain two sets of excitation spectra. The fluorescence peaks in each progression reveal the positions of the vibrational levels in one tautomeric species, relative to its own origins $|1, 0, (1)\rangle$ or $|1, 0, (2)\rangle$.* As we will be utilizing these levels in the studies of the relaxation processes, we list them in table 3.3.

Several points should be noted with respect to this table: 1. the uncertainty in

* In the future, we use $|l, m, (n)\rangle$ to represent the mth vibrational state on lth electronic singlet state. (n) indicates the type of tautomer.

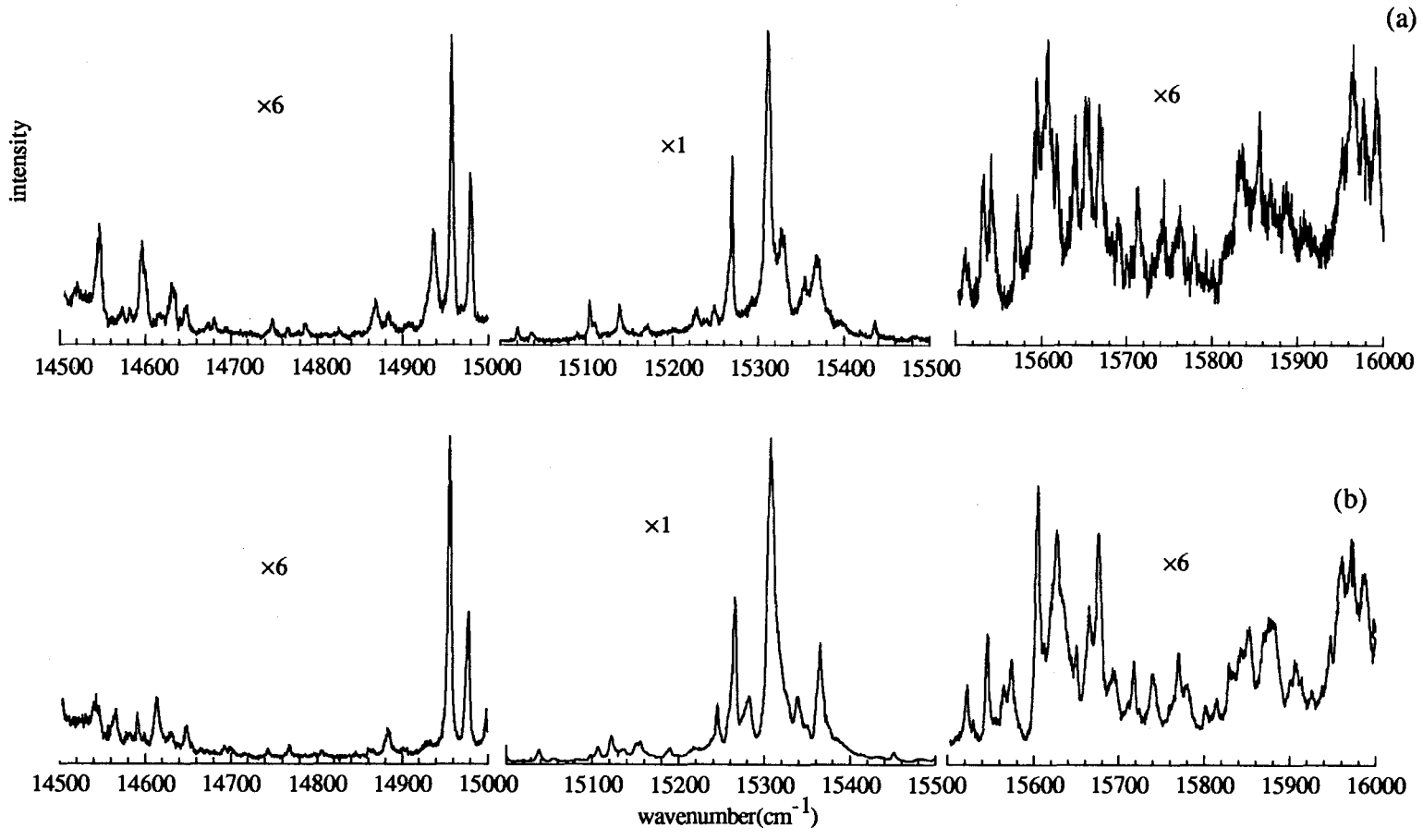

Figure 3.4 (a), (b) Fluorescence-excitation spectra of TBH_2Pc in hexadecane matrix. Laser swept the 14500 ~16000cm^{-1} frequency region, and fluorescence signals were monitored at (a) 14415cm^{-1} (b) 14436cm^{-1}.

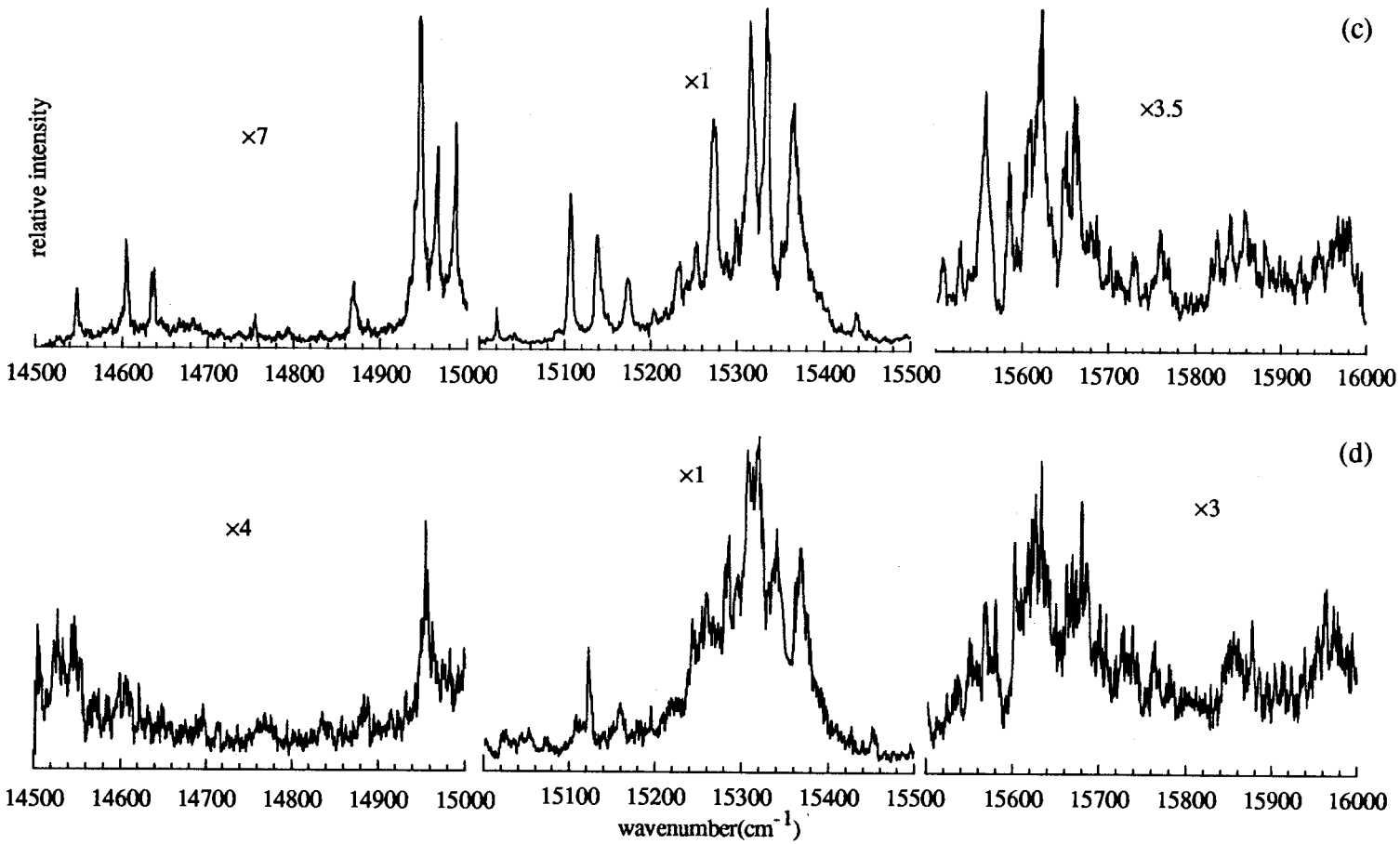

Figure 3.4 (a), (b) Fluorescence-excitation spectra of TBH_2Pc in pentadecane matrix. Laser swept the 14500 ~16000cm^{-1} frequency region, and fluorescence signals were monitored at (c) 14425cm^{-1} (d) 14440cm^{-1}

Table 3.3 Vibrational Energy Levels Relative to the $S_1^{(1)}$ and $S_1^{(2)}$ of TBH_2Pc in Hexadecane and Pentadecane

in hexadecane		in pentadecane	
$S_1^{(1)}$ (14436cm^{-1})	$S_1^{(2)}$ (14415cm^{-1})	$S_1^{(1)}$ (14440cm^{-1})	$S_1^{(2)}$ (14425cm^{-1})
103	101	104	101
128	127	129	124
142	142?	143	
151	153		
159	161	160	162
174	175	178	179
191	197	191	
209	211	209	209
228	228		
152	251?		251?
259	260	255	
303			
328	328	329	331
	366		368
	406	395?	405
443	447	445	444
	463		
516	516	515	518
538	537	538	538
559	559	559	560
598	600		597
614	616	613	615?
644			
658			
667	669	667	
682	684	682	684
716	719	719	714
750	752	752	749
805	808	804	809
825	828	822	828
844	849	847	847

Table 3.3 Continued

in hexadecane		in pentadecane	
$S_1^{(1)}$ (14436cm^{-1})	$S_1^{(2)}$ (14415cm^{-1})	$S_1^{(1)}$ (14440cm^{-1})	$S_1^{(2)}$ (14425cm^{-1})
901	904	901	906
925	930	927	
	947		
1013	1015	1014	1014
1059		1059	
1083		1091?	1083
1106	1110	1109	1106
1127	1129	1127	1132
1135	1138	1137	
1164	1167		
1187	1187	1188	1187
	1201		1200
1210	1210		
1227	1230	1228	1227
1231	1235	1232	1235
1258	1263	1259	1263?
1278	1280		1278?
1302	1302	1300	1303
1332	1333	1330	1335
1345	1350	1342	
1364	1368		
1376	1380		
1390	1387		
	1402		1401
1414	1414	1414	1415
1440	1440	1440	1435
1471	1468	1471	
1487	1490	1484	
1507		1507	
1522		1523	1519?
1532	1533	1532	
1545	1546		1546?

determining the peak positions not only depends on the accuracy of the instruments but also the width of the peaks. For most of them we estimated the uncertainty to be $\pm 2cm^{-1}$, but for some wider ones this may be up to $4\sim5cm^{-1}$; 2. excitation spectra do not provide information of the energy differences between |1, 0, (1) ⟩and |1, 0, (2) ⟩, |0, 0, (1) ⟩ and |0, 0, (2) ⟩ (i.e. the Δ_2 and Δ_1 in figure 1.5, page10). Just as the fluorescence spectra, they only provide information about the Δ_2-Δ_1; 3. the apparently strong $S_1^{(1)}$+867cm^{-1} and $S_1^{(2)}$+891cm^{-1} are excluded in the table, they are considered to be the vibrational levels of $S_2^{(1)}$ and $S_2^{(2)}$[52]. Above the $S_2^{(1)}$ and $S_2^{(2)}$ there will be overlappings of vibrational levels that belong to S_1 and S_2 ; 4. the number of vibration levels that appear in the spectra of TBH_2Pc in hexadecane is more than that in pentadecane. We believe this is a further indication that hexadecane holds the TBH_2Pc more firmly than pentadecane does, based on the greater molecular distortion leading to the lifting of more degeneracies in the vibration levels. This effect can also be seen when comparing the excitation spectra of H_2Pc obtained in a free jet[59] and in a Shpol'skii matrix[51]. The free jet method is considered to be virtually free from environmental effects and there are indeed more vibrational levels reported in [51] than in [59].

To summarize this section: the fluorescence and excitation spectra of TBH_2Pc, provide clear evidence that hexadecane is the most suitable solvent for the TBH_2Pc molecule to form a Shpol'skii matrix. This agrees in general with our prediction. Any slight discrepancy will be mainly the result of ignorance about the modification of the molecular dimension when appending the tertiary butyl groups to H_2Pc, as well as ignorance of the guest-host interactions. The work reported in next section was done with TBH_2Pc incorporated in hexadecane with a concentration of 10^{-4}M unless otherwise specified.

3.2 MILLISECOND RELAXATION PROCESSES AND INTERSYSTEM CROSSING

The radiative lifetime of a typical molecular excited singlet state is of the order of 1 - 10 nanosecond. Upon monochromatic excitation, the fluorescence intensity of the molecule will quickly reach equilibrium within this time interval, after the light source has been switched on. The fluorescence intensity depends on the quantum yield of this molecular level. However, different fluorescence behavior was observed in TBH_2Pc. When it was excited to a vibrational level of its tautomer(2)(e.g.$S_1^{(2)}$+516cm-^{1}), the 0-0 fluorescence of this tautomer first reached its maximum, then exponentially declined to equilibrium intensity within a time scale of hundreds of milliseconds(figure 3.5). As this phenomenon is resembling that observed in studies of ruby[3], we recognized that there must exist an intermediate energy level with a relatively long lifetime. This level acts as a reservoir, which receives a fraction of the excited population. As a consequence the initial ground state population $N_0(t = 0)$ exceeds that in steady state $N_0(t = \infty)$.

3. 2. 1 Simplified Three-level Dynamic Model

A realistic dynamic model of TBH_2Pc luminescence would involve many energy levels. But we can simplify this complex physical system by a three-level model. In figure 3.6, $|G\rangle$, $|E\rangle$ and $|P\rangle$ represent the ground, excited and intermediate states respectively. It is obvious that the A is spontaneous emission rate which is of the order of 10^8 s^{-1}.* The stimulated absorption rate W is related to A through the Einstein relation

$$W = \rho B, \tag{3.1}$$

---

* Chen *et al*[60] showed that the excited state lifetimes of the two tautomers in H_2Pc are 6.3 and 3.7 ns, one expects there is no major difference between H_2Pc and TBH_2Pc as far as their excited life time are concerned[61].

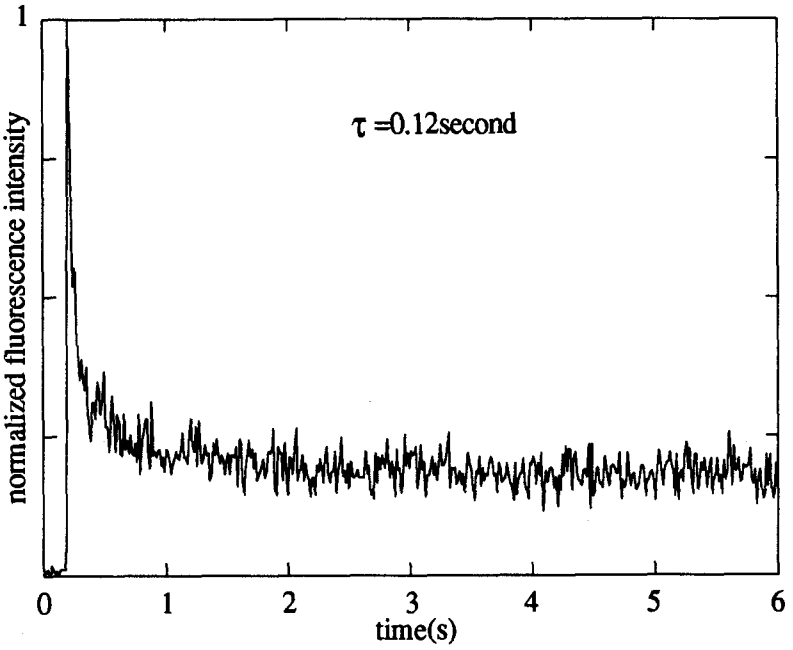

Figure 3.5 Time resolved 0-0 fluorescence behavior of TBH_2Pc after abruptly irradiating the sample

The excitation wavelength is $S_1^{(2)}$+516cm^{-1}

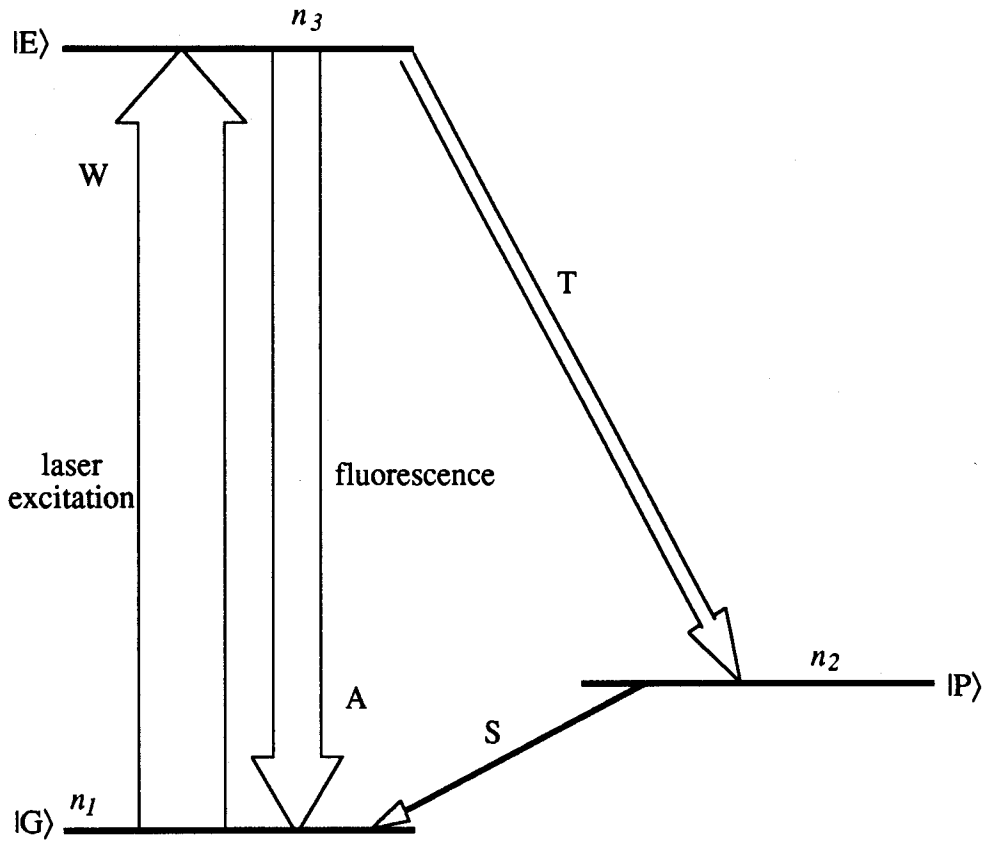

Figure 3.6. Simplified energy diagram of TBH_2Pc. $|G\rangle$ is $S_0^{(2)}$, $|E\rangle$ belongs to $S^{(2)}$, and $|P\rangle$ is an intermediate level whose status is currently not known.

$$B = \frac{c^3}{8\pi h\nu^3}A \sim 10^{13}A. \tag{3.2}$$

If the laser power is P = 100mW, the laser band width $\Delta\nu \approx 2\text{cm}^{-1}$ and cross section of the beam $\sigma \approx 10^{-6}\text{m}^2$, this yields

$$\rho = \frac{P}{\sigma c \Delta\nu} \approx 10^{-15}\text{Jm}^{-3}\text{s}, \tag{3.3}$$

and

$$W = 10^{-15}\times 10^{-13}A \approx 10^{6}\text{s}^{-1}. \tag{3.4}$$

The characteristic time τ of fluorescence intensity reduction in figure 3.5 gives the approximate value of the relaxation rate T from excited state to the reservoir, $T \sim 10\text{s}^{-1}$; S is estimated to be $10^{-1.5}\text{s}^{-1}$ for reasons that are explained in the next section. The rate equations of this system are:

$$\frac{dn_3}{dt} = Wn_1 - (T + A)n_3 \tag{3.5}$$

$$\frac{dn_1}{dt} = An_3 + Sn_2 - Wn_1 \tag{3.6}$$

$$n_1 + n_2 + n_3 = N \tag{3.7}$$

where N is the total number of molecule under laser irradiation. Through substitution, equations (3.5) - (3.7) yield

$$\frac{d^2n_1}{dt^2} + (a + d)\frac{dn_1}{dt} + (ad + bc)n_1 = -dSN \tag{3.8}$$

where a = -S -W, b = A - S, c = W, d = -T - A.

Eqn. (3.8) has a standard solution

$$n_1 = C_1 e^{k_1 t} + C_2 e^{k_2 t} - \frac{dSN}{ad - bc} \tag{3.9}$$

in which

$$k_{1,2} = \frac{1}{2}\left[a + d \pm \sqrt{(a+d)^2 - 4(ad - bc)}\right]$$

$$\approx \frac{1}{2}[-W - A - T \pm (A + W)],$$

hence

$$k_1 \approx -W - A, \quad k_2 = -\frac{T}{2}. \tag{3.10}$$

The last term in eqn.(3.9) is a function of excitation power

$$-\frac{dSN}{ad - bc} = \frac{(T + A)SN}{ST + SA + WT + WS}$$

$$\approx \frac{AS}{AS + WT} N = f(W), \tag{3.11}$$

f(W) is the equilibrium ground state population which will be examined in the next section. According to our predefined values of *A*, *S*, *W*, *T*, we have $f(W) \sim 10^{-0.5}N$. Thus eqn.(3.9) becomes

$$n_1 \approx -C_1 e^{-(W+A)t} + C_2 e^{-\frac{T}{2}t} + f(W). \tag{3.12}$$

Similarly we can also find

$$n_3 = \frac{1}{b}\left(\frac{dn_1}{dt} - an_1 - SN\right)$$

$$\approx -C_1 e^{-(W+A)t} + \frac{W}{A} C_2 e^{-\frac{T}{2}t} + g(W) \tag{3.13}$$

where

$$g(W) = \frac{W}{A} f(W) \sim 10^{-1.5} N. \tag{3.14}$$

Imposing the initial conditions for n_1 and n_3:

$$n_3(0) = \alpha N \tag{3.15}$$

and

$$n_1(0) = (1-\alpha)N, \qquad (0< \alpha \leq 1) \tag{3.16}$$

we find

$$\begin{aligned} C_2 &\approx N - f(W) \\ &= h(W) \approx 10^{-0.2} N, \end{aligned} \tag{3.17}$$

$$C_1 \approx \left(\frac{W}{A} - \alpha\right) N. \tag{3.18}$$

Note that the first terms in eqns.(3.12) and (3.13) are too evanescent in our time scale of interest, so the double lifetime in eqn.(3.13) reduces to

$$n_3 = \frac{W}{A} h(W) e^{-\frac{T}{2}t} + g(W), \tag{3.19}$$

and the fluorescence intensity

$$\begin{aligned} I_F &= Ag(W) + Wh(W) e^{-\frac{T}{2}t} \\ &= W\left\{ f(W) + [N - f(W)] e^{-\frac{T}{2}t} \right\} \end{aligned} \tag{3.20}$$

consist of a stable and a decaying part. It is striking how closely the experimental data fit to eqn.(3.20). Several hundred trials with different experimental parameters (with each trial

containing 400 data points) constantly give >0.95 for the regression rate of the curve fitting. Moreover, we defined the equilibrium fluorescence intensity $I_s=Ag(W)$ and the fluorescence reduction $\delta=Wh(W)$. Given $g(W)\sim10^{-1.5}N$, $h(W)\sim10^{-0.2}N$, their theoretical ratio should be

$$\frac{\delta}{I_s} \approx 10^{0.5} \sim 3. \tag{3.21}$$

Our experimental result of $\frac{\delta}{I_s} = 3$ from figure 3.5 proves the correctness of the approximationt of W.

A fluorescence intensity equation was proposed in the study of the transformation processes of H_2Pc in an α-ClN and *n*-octane mixture[62], viz.

$$I = F\left[N_0 + (N - N_0)\exp\left(-\frac{t}{\tau}\right)\right] \tag{3.22}$$

where F is a function of laser power and oscillator strength of the states, N_0 is the equilibrium ground state population. Noting that by definition the N_0 in eqn.(3.22) corresponds to our $f(W)$. We soon identify F as precisely the stimulated excitation rate W. However, eqn.(3.20) does not agree with the modified form of eqn.(3.22) in principle[62], where the N_0 was claimed to be a linear function of time:

$$I = (n_0 - at) + \left[n - (n_0 - at)\right]\exp(-t/\tau). \tag{3.23}$$

Although eqn.(3.23) fits the experimental data better than eqn.(3.22), we stress that the mathematical formulation should not be the first consideration. Irrespective of H_2Pc or TBH_2Pc, under no circumstance should the population on certain energy states become

negative, which would the case in eqn.(3.23) after a certain period of time. Thus eqn.(3.23) can only be considered an approximation valid for relatively short time.

3. 2. 2 Millisecond Relaxation Mechanism

Table 3.4 gives the parameters characterizing the relaxation process on $S_1^{(2)}$+516cm^{-1}. Both fluorescence reduction and steady fluorescence intensity increase with the excitation power, but the pattern of the variation of $\frac{\delta}{I_s}$ does not resemble the linear one predicted by the model*.

Table 3.4 Fluorescence intensity and reduction as a function of excitation power.
$\nu_{exc} = S_1^{(2)}$+516cm^{-1}=14931cm^{-1}, $\nu_{fluore.}=S_1^{(2)}$ =14415cm^{-1}

Excitation Power (±1mW)	Steady State intensity I_s(count)	fluore. reduction δ(count)	τ (ms)
7	257±2	876±28	289±22
13	400±3	1736±37	245±14
25	575±12	2800±85	165±7
35	820±7	3838±83	142±7
44	1026±18	4880±82	139±10
59	1364±10	5560±76	119±7
90	———**	———**	129±7

This inconsistency leads to further speculation that the relaxation rates T and S may be

---

* From eqns.(3.11) to (3.20), it can be found that $\frac{\delta}{I_s}=\frac{WT}{AS}$, which is a linear function of W.

** Experiment of P=90mW was performed separately, its data are unable to be compared with others.

functions of excitation power. For this reason, the fluorescence reduction characteristic time τ under various excitation powers was measured. We found that the τ was rather susceptible to changes at low excitation power but was unresponsive to changes at high power. An empirical equation representing this relation is also given, namely

$$\frac{2}{T} = \tau = (0.12\pm 0.01) + (0.28\pm0.02)\exp(-\frac{P}{14\pm2}), \qquad (3.24)$$

where τ and P are in the units of second and mW respectively(fig.3.7). The saturated relaxation rate T_S, particularly for $S_1^{(2)}$+516cm^{-1}, was determined to be (16.3±0.2)s^{-1}. For some higher vibration levels, their T_S's were also determined. They are (12.5±0.8)s^{-1} for $S_1^{(2)}$+684cm^{-1}, (14.2±1.0)s^{-1} for $S_1^{(2)}$+719cm^{-1}, (13.3±1.8)s^{-1} for $S_1^{(2)}$+1333cm^{-1}, (15.4±2.4s)s^{-1} for $S_1^{(2)}$+1015cm^{-1}. This indifference of the relaxation rates to their excitation frequencies contradicts the conclusions drawn in the studies of H_2Pc[62] and TBH_2Pc[52], where T differs from one excitation frequency to the other. In addition, our τ=(0.16±0.1)s for $S_1^{(2)}$+684cm^{-1} does not correspond to the τ=90ms that quoted in [52] for the same level. It should be pointed out that if the statistical analysis is ignored, the high fluctuations in the measurement of parameters such as τ, δ, I_s can easily mislead one into incorrect conclusions. (In our experiments, considering that under some circumstances the percentage error due to the fluctuation was even higher than 100%, all trials were repeated at least ten times to ensure a higher degree of certainty).

For a molecule like TBH_2Pc, its complex energy level system provides many possible pathways for relaxation to ground state after excitation. These pathways can be single steps, but in most of the cases they will be combinations of single steps. We rule out pathways such as intermolecular interaction: the 1×10^{-4}M concentration yields the intermolecular distance of ~30nm, which is far greater than the diameter of the molecule. This makes it likely that the guest molecules are well isolated from one another in the solvent

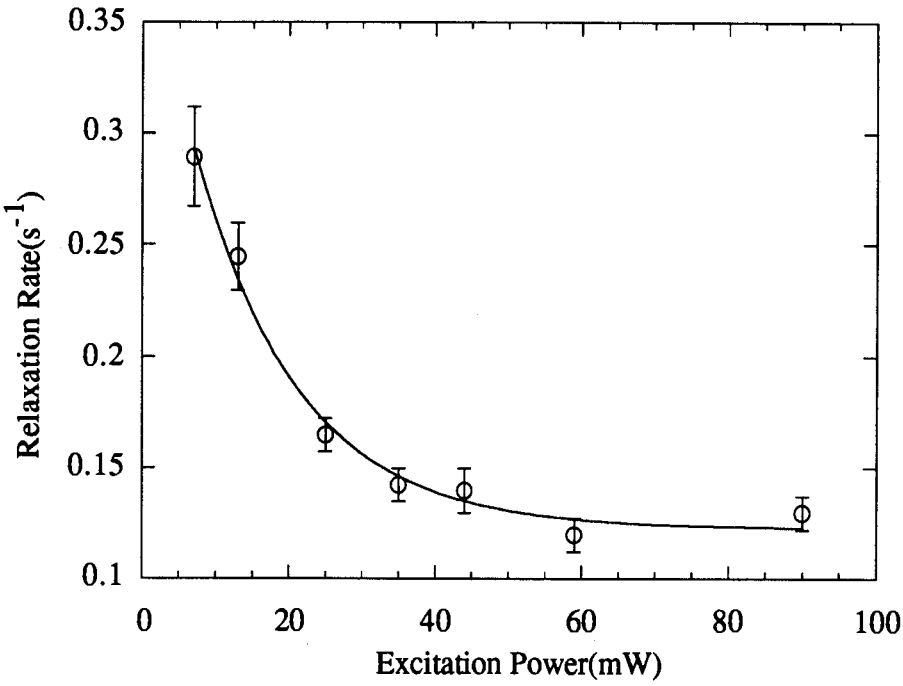

Figure 3.7 Millisecond relaxation rate as a function of excitation power

matrix. An additional confirmation of this comes from that the experimental values of T_S for $S_1^{(2)}$+684cm^{-1} and $S_1^{(2)}$+719cm^{-1} measured with a concentration of 1×10^{-5}M. They are respectively (16.6±6.9)s^{-1} and (15.4±7.9)s^{-1}, i.e. virtually no difference from those values at a concentration of 1×10^{-4}M. Phonon assisted processes are also deliberately neglected, as figure 3.4 shows that this interaction is already minimized in hexadecane. For the remaining purely *intramolecular* processes, the first step of the molecular relaxation from the *i*th vibrational level(say, $|1,i,(2)\rangle$) may be in such a way that the two inner protons switch their positions by tunnelling through the potential barrier in the excited state, so that the molecule shifts from one tautomeric form to the other; it may also undertake the route of radiationless internal conversion* . The probability of the tunnelling effect can not be presumed to be small, because the height and shape of the potential barrier in the S_1 state is not known. To recognize the influence of tunnelling, we examine the 0-0 fluorescence spectra of the vibrational levels($S_1^{(2)}$+516cm^{-1}, $S_1^{(2)}$+684cm^{-1}, $S_1^{(2)}$+719cm^{-1}, $S_1^{(2)}$+1015cm^{-1}, $S_1^{(2)}$+1333cm^{-1}). These levels unambiguously exhibit the millisecond relaxation effect and the fluorescences of tautomer (1) can always be found in the spectra(fig.3.8). Note that these five levels are rather "isolated" ones, that is they do not coincide with any levels belonging to tautomer (1). Hence the very existence of the fluorescence of tautomer (1) in these cases can not be interpreted as incidental excitation of the tautomer (1). Rather, it should be interpreted as the results of light induced proton tunnelling. Note that since the ratio of the 0-0 fluorescence $f^{(1)}/f^{(2)}$ are all smaller than unity, we are convinced that the tunnelling effect plays only minor role. From table 3.5, the ratio $f^{(1)}/f^{(2)}$ approaches closer to unity as the excited vibrational level become higher and higher. This fact further confirms our proton tunnelling hypothesis, because under any circumstance the thickness of the potential barrier should become thinner as the energy increases, so that it will be

---

* Internal conversion can even occur as an intramolecular process between states of the same or different multiplicity in the absence of solvent interaction. See, for example, [63].

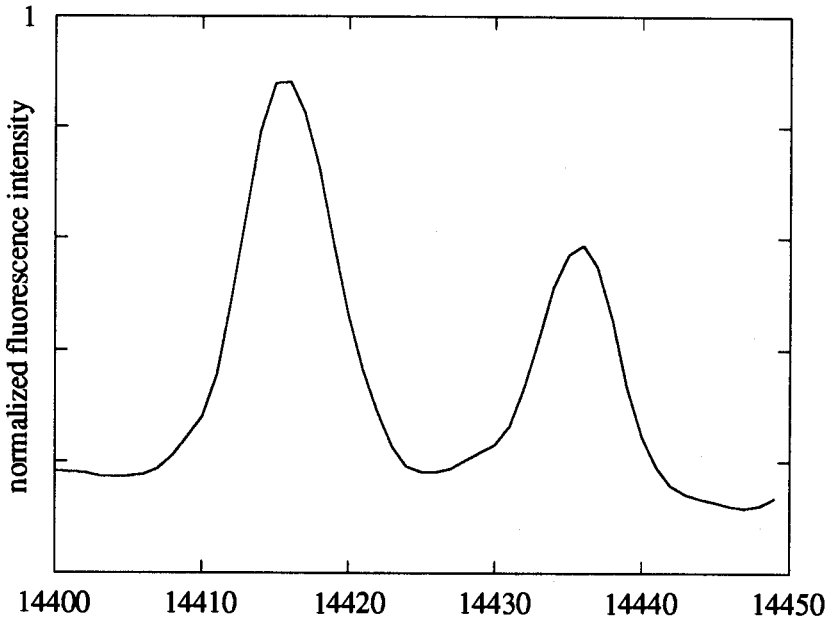

Figure 3.8. 0-0 fluorescence of the two tautomers of TBH_2Pc. The excitation wavelength is $S_1^{(2)} + 1015cm^{-1}$. Their intensity ratio is $f^{(1)}/f^{(2)} = 0.71$.

easier for the protons to penetrate.

Table 3.5 Ratio of 0-0 fluorescence intensities of the two tautomers under different excitations

excitation levels $S_1^{(2)}$+	0-0 fluore. inten. ratio $f^{(1)}/f^{(2)}$
516cm^{-1}	0.32±0.01
684cm^{-1}	0.71±0.01
719cm^{-1}	0.79±0.02
1015cm^{-1}	0.82±0.01
1333cm^{-1}	0.89±0.02

Similar to the observations in H_2Pc [62], most of the vibrational levels of TBH_2Pc that exhibit millisecond relaxation phenomena are low lying ones. The lower the level, the more salient the millisecond relaxation feature. Moreover, it is worth to mention that millisecond relaxation phenomena are also observable in 0-1 fluorescence with 0-0 excitation. Recall that the energy splitting of the two tautomers on S_1 state is ~20cm^{-1}, it makes it very difficult for a proton to tunnel through the potential barrier and occupy the higher level at the same time. All these imply that although a fraction of the excited population relaxes to $S_1^{(1)}$ through proton tunnelling, the tunnelling on the excited states itself is not responsible for the millisecond processes. As we have mentioned that the saturated rate T_S is insensitive to the excitation wavelength, it is very probable that the first step of the millisecond relaxation process is that the molecule is internally converted to one level, regardless of which vibrational level is excited. This level is, without speculation, the $|1, 0, (2)\rangle$ state.

So far we have not identified the transition that represents the T process in the three-

level model. The foregoing internal conversion rate is several orders faster than the spontaneous emission rate and it appears to be certain that the millisecond process must occur in the subsequent steps of the relaxation. The radiative process of $S_0^{(1)} \leftarrow S_1^{(2)}$ is restricted by the Franck-Condon principle, hence there are only two alternatives for the TBH_2Pc molecule to relax from the vibrationless level of S_1 to S_0. The first alternative is to cross from $|1, 0, (2)\rangle$ to $S_0^{(1)}$ through internal conversion, as a result of vibronic coupling with the high lying vibrational states of S_0; while the second one can be from $|1, 0, (2)\rangle$ to the lowest metastable triplet state via intersystem crossing. The present experiments do not permit us to draw a precise picture of the pathway. However, it seems to us that the intersystem crossing should dominate the millisecond process, based on the following consideration: from the transition rate point of view, the typical internal conversion rate of $S_0 \leftarrow S_1$ of organic molecules is $10^5 \sim 10^7 s^{-1}$[63], we believe TBH_2Pc is with no exception. If the majority of population are supposed to relax to either $S_0^{(1)}$ or $S_0^{(2)}$ with this fast rate, it will be impossible to satisfy the requirement of the existence of two slow processes in the three-level model. On the other hand, although the phosphorescence of TBH_2Pc has not been observed, it does not imply that there is no triplet state. Besides phosphorescence, there also occurs internal conversion to provide a depletion channel for the triplet state. Both rates of phosphorescence and internal conversion from triplet state are expected to range from $10^{-1} \sim 10^3 s^{-1}$, which would coincide with the rate T in the three-level model. In the study of the photochemical isomerization of free base porphin(H_2P) in *n*-octane matrix at 4.2K, Völker and van der Waals[6] determined the $T_0 \longrightarrow S_0$ decay rate to be $92s^{-1}$(and $42s^{-1}$ for deuterium porphyrin). This is of the same order of magnitude as the rate T in TBH_2Pc, supporting our hypothesis that intersystem crossing from T_0 toS_0 is responsible for the millisecond mechanism. Völker *et al* also stated that the high quantum yield of the triplet state, which was measured to be least 90 percent[64], was part of the reason for intersystem crossing being a path in the phototransformation. In our case a high phosphorescence yield is not a necessary premise for the observation of the millisecond process

in TBH_2Pc. Even a small phosphorescence yield say, one percent of that of fluorescence, would give an intersystem crossing rate still of the order of $10^6 s^{-1}$ which is fast enough to compete with the fluorescence process and populate the triplet state. Moreover, the fluorescence quantum yield of TBH_2Pc is known to be lower than that of H_2Pc(which very close to unity[61]) and hence intersystem crossing may be more likely than in H_2Pc. Electron spin resonance experiment showed that for free base porphin the two lowest triplet states are of orbital symmetries B_{2u} and B_{3u} respectively[65]. Völker *et al*[6] proposed that vibronic coupling between these lowest triplet states induced the transformation between the two species of H_2P, owing to the fact that the vibronic coupling occured via b_{1g} vibrations, as well as that the libration of the inner protons about z-axis(perpendicular to the molecular plane) is a type of proton displacement that only occured in b_{1g} normal modes. There has not been any ESR experiment for the TBH_2Pc molecule to indicate what symmetries the lowest triplet state should possess. But if we accept the facts that both TBH_2Pc and H_2P have the same D_{2h} symmetry when they are incorporated in solid matrix, as well as that the optical properties of the porphyrin-like compounds are largely determined by the central porphin ring, then we may have confidence in asserting that similar vibronic coupling will also occur in TBH_2Pc, so that it can induce the transformation of tautomers. Furthermore, when the vibrational level of the triplet states is high, one may no longer speak of the libration of the two inner protons in a well-defined potential well, since the motion of the protons can no longer be separated from that of electrons. In this case, there will be a finite probability for the type (2) tautomer of TBH_2Pc to cross from $|1, 0, (2)\rangle$ to $T_1^{(1)}$ with a rotation of the two protons by $\pi/2$. Eventually, the radiation or radiationless transitions from the metastable$T_1^{(1)}$ may play a role in the millisecond process.

Before leaving this section, we like to outline all possible relaxation pathways of TBH_2Pc to avoid confusion of the readers. These correspondingly are:

(a) vibrational relaxation, $10^{11} \sim 10^{14} s^{-1}$.

(b) proton tunnelling, deplete a fraction of excited population.

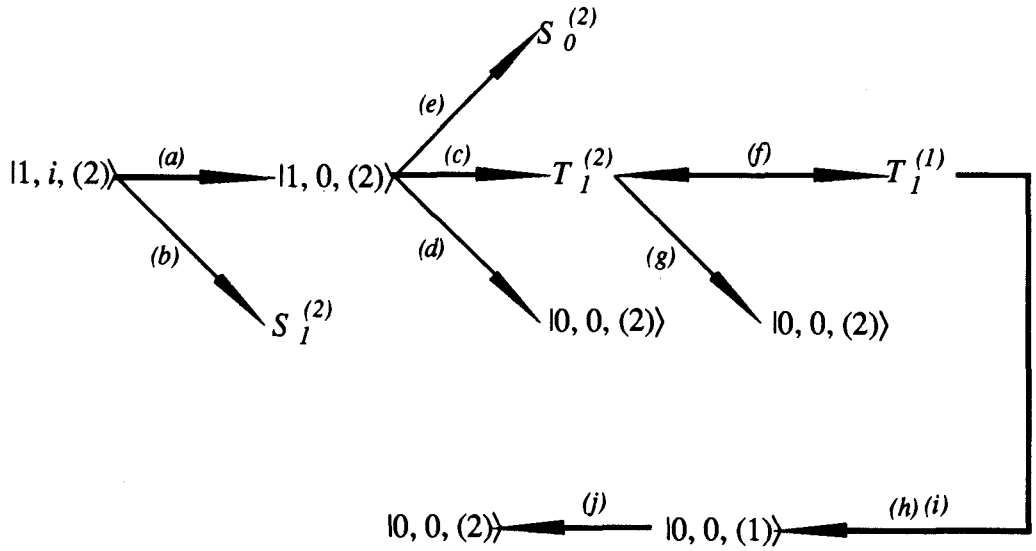

(c) intersystem crossing, whose rate is $10^6 \sim 10^7 s^{-1}$ depending on quantum yield, but it does not affect the observation of the millisecond processes.

(d) fluorescence, most population goes through this channel.

(e) internal conversion, whose rate may range from $10^5 \sim 10^7 s^{-1}$.(f) transformation to tautomeric species again due to the vibronic coupling in the triplet state

(g) phosphorescence and internal conversion, $10^{-1} \sim 10^3 s^{-1}$.

(h), (i) phosphorescence and internal conversion. Responsible for millisecond process. The *experimental value* of their combination rate is $(14.3 \pm 0.8) s^{-1}$.

(j) mechanism and rate are currently unknown, must be very slow according to the model.

In the above diagram only the one(marked by bold line) among the diverse routes is responsible for the millisecond process. Unfortunately, we are presently not able to

determine which one in routes (h) and (i) is more favorable in the competition, as this requires more sophisticated phosphorescence signal detections.

3.3 NONRADIATIVE TRANSITION BETWEEN GROUND STATES, BOTTLENECK EFFECT

The fluorescence reduction portrayed in figure 3.5 was acquired by abruptly irradiating with laser on to the sample that *had no previous excitation history.* If one switches the excitation on and off alternately, one will notice that the fluorescence reduction δ retains the characteristics of the dark history, that is, it changes as the function of dark time. Clearly, even with the absence of excitation the molecule still undergoes a dynamic process. Figure 3.9 illustrates the 0-0 fluorescence reduction effect with different dark pauses before the $S_1^{(2)}$+516cm^{-1} excitation turned on (prior to the dark pause the molecule was in equilibrium state under laser irradiation). Starting with fig.3.9(a) with 5 seconds of dark time to fig.3.9(f) with 70 seconds of dark time, the reduction δ rises by six times, and the change eventually slows down and saturates as the dark time exceeds one minute. On the other hand, the millisecond characteristic time remains 0.14s unchanged with the dark time. Comparing this with the other molecular relaxation processes, this process is rather slow, it can be looked upon as a bottleneck, so named as it controls the population that is returning to the ground state when the upper level is populated. Before we proceed to discuss the mechanism of the bottleneck phenomenon, we like to extend the derivation in the preceding section as this may explain our observations.

3. 3. 1. The Three-level Dynamic Model (continued)

The equations describing the equilibrium state under excitation are eqns(3.5) and

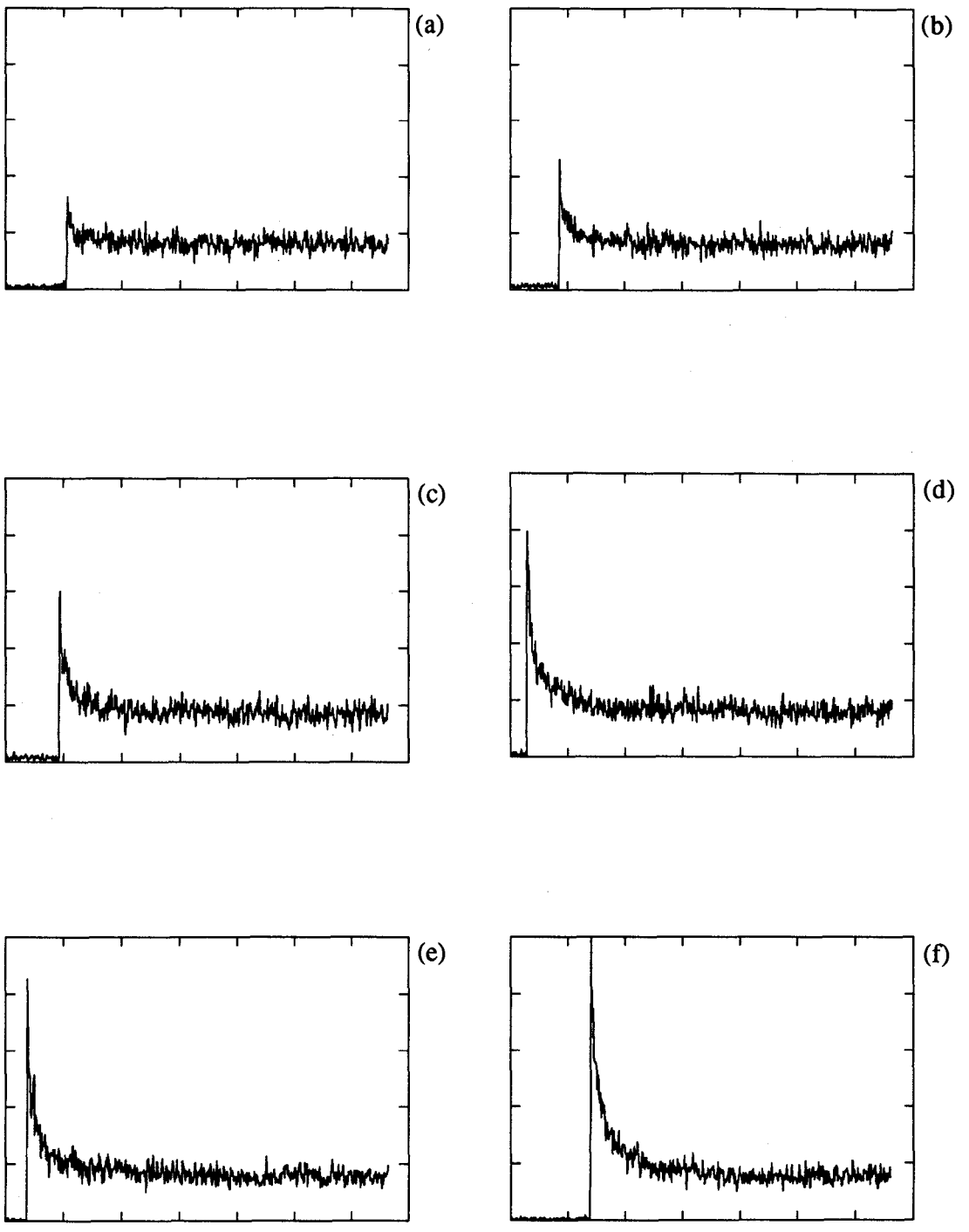

Figure 3.9 Different fluorescence reductions characterize the dark history prior to the excitation($S_1^{(2)}$+516cm^{-1}). The dark times for each picture are, from (a) to (f), 5s, 10s, 20s, 30s, 40s, 70s. The x- and y-axes are time and relative fluorescence intensity respectively.

(3.6) with their left-hand-sides zero, while eqn.(3.7) remains as is. Solving these steady state equations yields

$$n_3 \approx \frac{SW}{AS+WT}N = g(W), \tag{3.25}$$

$$n_2 \approx \frac{WT}{AS+WT}N = h(W), \tag{3.26}$$

$$n_1 \approx \frac{AS}{AS+WT}N = f(W), \tag{3.27}$$

So the f, g, h that appeared frequently in the derivations in the preceding section represent the equilibrium populations on each level under steady state excitation. Directly from eqns.(3.6) and (3.7) we are also able to write down the dynamic equations during the dark pause:

$$\frac{dn_3}{dt'} = -(T+A)n_3, \tag{3.28}$$

$$\frac{dn_1}{dt'} = An_3 + Sn_2, \tag{3.29}$$

$$n_1 + n_2 + n_3 = N, \tag{3.7}$$

where the t' starts at the moment when the excitation shuts off. Immediately we find

$$n_3 = D_1 e^{-(T+A)t'} \approx D_1 e^{-At'}, \tag{3.30}$$

$$n_1 = e^{-St'}\left[\frac{AD_1}{S-A}e^{-(S-A)t'} + Ne^{-St'} + D_2\right]$$

$$\approx -D_1 e^{-At'} + D_2 e^{-St'} + N. \tag{3.31}$$

To determine the constants D_1 and D_2, let

$$n_1(0) = f(W), \tag{3.32}$$

$$n_3(0) = g(W), \tag{3.33}$$

then

$$D_1 = g(W), \tag{3.34}$$

$$D_2 = f(W) + g(W) - N \approx -h(W), \tag{3.35}$$

so that

$$n_1 \approx N - h(W)e^{-St'}. \tag{3.36}$$

After renewed irradiation of the sample by the laser, the system is again governed by eqns(3.5) to (3.7), but the initial conditions (3.15) and (3.16) need now be modified to

$$n_3(0) = \alpha\left(N - he^{-St'}\right), \tag{3.37}$$

and

$$n_1(0) = (1-\alpha)\left(N - he^{-St'}\right). \tag{3.38}$$

using eqn.(3.13)

$$n_3 = -C_1 e^{-(W+A)t} + \frac{W}{A} C_2 e^{-\frac{T}{2}t} + g(W)$$

$$\approx \frac{W}{A} h\left(1 - he^{-St'}\right) e^{-\frac{T}{2}t} + g(W). \tag{3.39}$$

Similar to eqn.(3.20), the fluorescence intensity is $I_F = An_3$ and the reduction will be

$$\delta(t') = Wh(1 - e^{-St'}), \tag{3.40}$$

which is an exponential function of time. What Eqns.(3.39) and (3.40) imply is clear: the dark time will not alter the millisecond relaxation rate but the fluorescence reduction; the bottleneck rate S can be directly obtained from the relation between fluorescence reduction and dark time. Figure 3.10 shows a set of experimental data (excitation = $S_1^{(2)}$ + 516cm^{-1}) which is fitted by eqn.(3.40), and the bottleneck rate is found to be $(3.1 \pm 0.2)\times10^{-2}$s^{-1}.

Just because the bottleneck process persists considerably longer than the other processes, its rate S should be insensitive to excitation wavelength. A more precise value of S can be determined by averaging those acquired from different excitations, which are tabulated in table 3.6.

Table 3.6 Bottleneck Relaxation Rates for Different Excitations

Excitation ($S_1^{(2)}$ +)	Relaxation Rate($\times10^{-2}$s^{-1})	Regression Rate for Curve Fitting
516cm^{-1}	3.1±0.2	1.00
684cm^{-1}	3.0±0.4	0.99
719cm^{-1}	2.7±0.3	0.99
1015cm^{-1}	3.3±0.6	0.98
1333cm^{-1}	2.9±0.3	0.99
Average	**3.0±0.2**	—

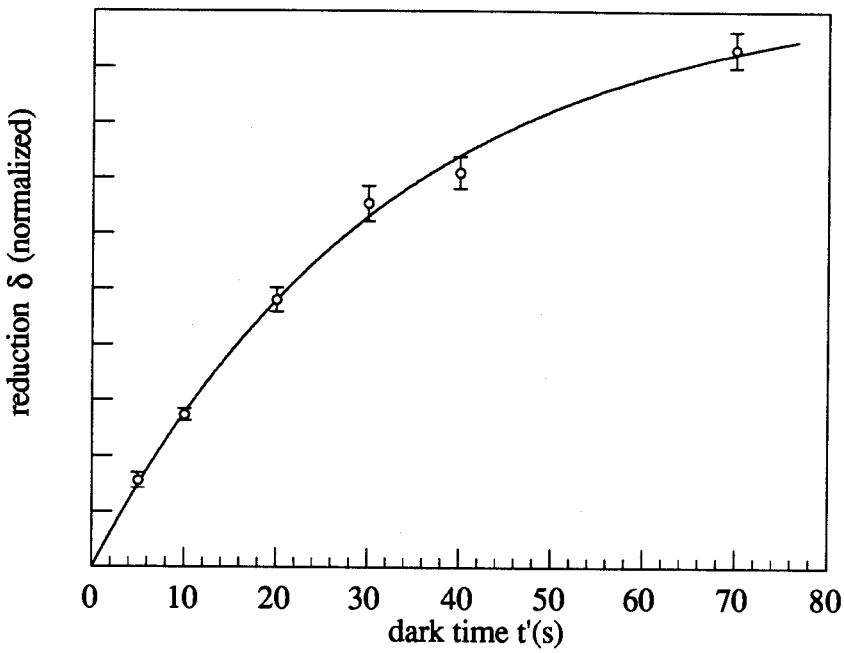

Figure 3.10. Dark time dependence of fluorescence reduction based on data in fig.3.9. Curve is fitted by eqn.(3.40). Here $S = (3.1 \pm 0.2)10^{-2} sec^{-1}$ and regression rate is 0.99.

3. 3. 2 WKB Approximation in Proton Tunnelling

It has been pointed out, at the end of the section 3.2, that the millisecond process is substantially the transition from the lowest triplet state to the ground state. If the bottleneck process follows subsequently to this transition, it must occur between the ground states. Radiation processes are unlikely to be involved. But the molecule, for instance, can change its proton position by tunnelling through the potential barrier in a nonradiative relaxation process. If such hypothesis turns out to be true, the experimental bottleneck rate should directly relate to the proton tunnelling rate in the ground state.

The semiclassical WKB approximation method is used to estimate the proton tunnelling rate, owing to the simplicity of the procedure it involved, as well as the applicability of the method our one dimensional problem. Solving for the protons bounded in the TBH_2Pc molecule is in principle a many-body problem, for the full Hamiltonian of the molecule contains not only the potentials describing the interactions between the massive atomic nuclei, but also potentials describing the electron-electron interaction. This type of extremely complex situation can only be solved in approximation based on some assumptions, which lead to the simplification of the many body problem to that of an independent proton one. The assumptions we use are:

1. All interatomic and interelectronic interaction are represented by an effective molecular potential $V(\theta)$, which appears in periodic well configuration with barrier height V_0, period $\frac{\pi}{2}$ and the degree of asymmetry Δ(the energy difference of the two minima).

2. We focus on the motion of the two inner protons and assume these to be librations in the effective molecular potential $V(\theta)$

The conclusion arrived at from the above assumptions is of crucial significance: The coupled protons now have their own wave function that can be described by the time independent Schrödinger equation. We start the WKB approximation by the quantization rule[66]

$$\int_b^c p(\theta)d\theta = \left(n+\frac{1}{2}\right)\hbar\pi, \tag{3.41}$$

in which $p(\theta) = \sqrt{2I(E - V)}$ and $n = 0, 1, 2, 3\ldots$, and b, c are turning points(Fig.3.11). Due to the fact that the inner protons are strongly coupled, they act as a librating dumb-bell. Thus the moment of inertia $I=2mr^2$. The tunnelling probability then depends on the real part of the proton wave function $\psi(\theta)$ that spreads in the $\theta < a$ region(we only discuss $-\frac{\pi}{2} < \theta < \frac{\pi}{2}$ region):

$$\psi(\theta)\big|_{\theta<a} = \exp\left(-\frac{1}{\hbar}\int_a^b |p|\, d\theta\right). \tag{3.42}$$

Hence the transmission coefficient for the nth eigenvalue can be expressed as the square of the Re(ψ)

$$D_n = \exp\left(-\frac{2}{\hbar}\int_a^b |p|\, d\theta\right), \tag{3.43}$$

The probability per unit time of emergence from well (1) to well (2) is equal to vD[67]. In practice, the periodic nature of the potential well (not seen in fig.3.11) makes the tunnelling rate equal to twice the above probability, i.e. $S_n=2D_n\nu_n$.

There is no unique mathematical formulation regarding the periodic well molecular

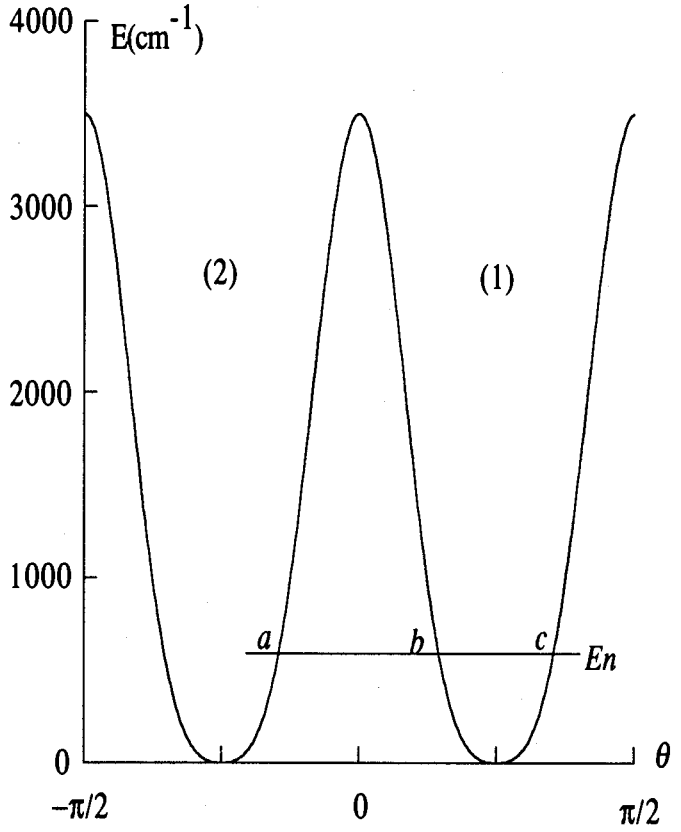

Figure 3.11 Schematic of effective molecular potential with V_0=3500cm^{-1}, $\Delta \approx 0$, $\sigma = 0.082\,\pi$. (see main text for the definitions of the parameters)

potential configuration of TBH_2Pc, but we found empirically that a Gaussian barrier modified by a cosine function is the most suitable among the different periodic configurations. That is:

$$V(\theta) = \frac{V_0}{2}(1+\cos 4\theta)\exp\left[-\frac{(\theta-\frac{n\pi}{2})^2}{2\sigma^2}\right], \tag{3.44}$$

where the factor of four guarantees the potential zero at $\theta=\pm\pi/4$. From the absorption spectrum of TBH_2Pc in the same crystal[68] at 1.5K, we convert the ratio of the two absorption peaks ($S_o^{(2)} : S_o^{(1)} = 6 : 1$) to the energy difference of $\Delta \sim 2cm^{-1}$, thus it is purposely neglected from the formulation. Direct measurements of the barrier height V_0 are not available at present; but only NMR experiments on the related molecule tetraphenylporphrin showed a barrier height of $3500cm^{-1}$. So we expect a comparable barrier in TBH_2Pc[23]. There is even larger uncertainty in the estimation of the moment of inertia I: From table 3.1, one can calculate the diagonal length between the two aza-nitrogen atoms to be 0.38nm. But the two inner protons are not visible by X-ray diffraction. If one takes the N-H bond length to be ~0.1nm, the radius of the proton dumb-bell r can be 0.1nm at two energy minimum positions. However, when the protons are situated at any position other than the two energy minima, the r will be considerably longer. In fact the libration path of the protons may not necessarily lie on the molecular plane. Therefore we estimate the *average* radius of the proton dumb-bell to be 0.12±0.01nm. With the values of V_0, r, and the barrier width σ, the integral equation (3.41) can be numerically solved with arbitrary precision. At 0K the particle only occupies the lowest eigenstate, thus the tunnelling rate is acquired by substituting E_0 into eqn.(3.43). Numerical calculation results are demonstrated in figure 3.12, where many combinations of

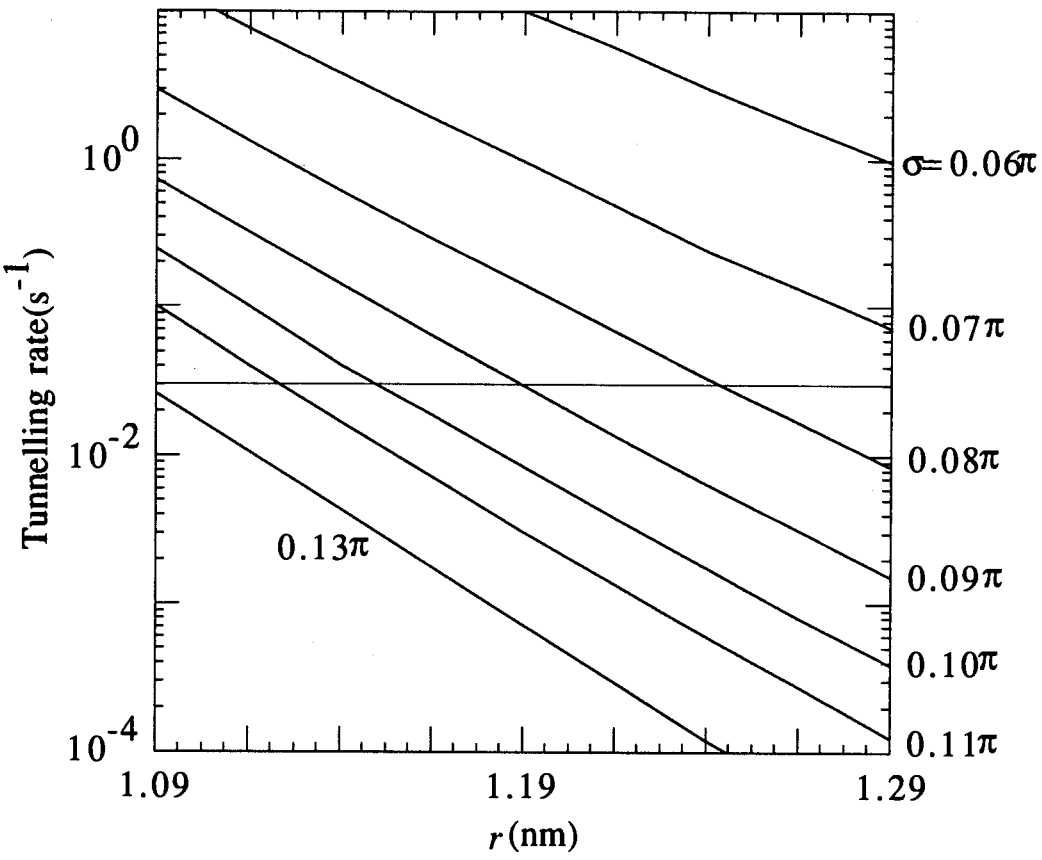

Figure 3.12 Numerical results of proton tunnelling rate at T =0K. The horizontal line is the experimental value at 4.2K, so the intersects represent the possible combinations of r and σ.

r and σ can result in the experimental tunnelling rate, namely $3.0\times10^{-2}s^{-1}$. Since r has higher degree of certainty we conclude from the tunnelling at 4.2K* that the σ must be within the range of 0.075π to 0.13π.

In the case of nonzero temperature, the tunnelling situation is slightly more complicated.The total rate is obtained by summing up the weighted contributions of each state and it becomes a function of temperature

$$S(T) = \frac{Tr(v_n D_n \rho)}{Z} \tag{3.45}$$

where

$$Z = Tr\rho = \sum_{n=0}^{\infty} \exp\left(-\frac{E_n}{kT}\right) \tag{3.46}$$

is a partition function of the canonical ensemble. In practice, the convergence of the above equation allows us to truncate finite terms from it within a certain temperature range.

Figure 3.13 shows the experimental temperature dependence of the proton tunnelling rate S. It is worth noting that this experimental temperature dependence will narrow further the possible values of r and σ. This happens because that while there is indeed a wide range of r and σ which results in measured tunnelling rate at 4.2K, only a sole combination gives the experimental tunnelling rate at 77K, namely $(0.34\pm0.02)s^{-1}$. In other words, this particular combination, r=0.12nm, $\sigma=0.082\pi$, provides a unique set of

* One should note that there is virtually no difference between 0K and 4.2K in terms of tunnelling rate.

eigenvalues which results in measured tunnelling rate. The theoretical curve in figure 3.13 is the result of $S(T)$ by taking the first ten eigenstates in table 3.7.

It is not surprising that even this theoretical curve deviates still to some extend from the experimental one. While we consider that proton tunnelling plays the main role in the tautomeric transformation, we do not rule out other possible mechanisms(such as phonon

Table 3.7 The First Ten Eigenstates in the Proposed Gaussian-Cosine Potential Configuration.

$80cm^{-1}$	$876cm^{-1}$
$239cm^{-1}$	$1034cm^{-1}$
$398cm^{-1}$	$1194cm^{-1}$
$557cm^{-1}$	$1353cm^{-1}$
$716cm^{-1}$	$1513cm^{-1}$

assisted process). In addition, the experimental data between 20K to 50K have the highest uncertainty: this may also contribute to the deviation.

Finally, it is interesting to compare the bottleneck effect of TBH_2Pc in a pentadecane matrix to that in hexadecane. We did not investigate this aspect very extensively. However, data appear that the bottleneck effect in a pentadecane matrix persist far longer than in hexadecane. In the foregoing derivation we have seen that the tunnelling rate is extremely susceptible to the potential barrier width and height. It is unlikely that the barrier height for the same molecule varies in different solvents, but it is possible that the barrier width changes when the molecule is subjected to the stress from the solvent matrix. If TBH_2Pc receives less stress in the pentadecane matrix, its molecular potential width will likely be larger, so that it causes a longer bottleneck time. This would be in general agreement with the conclusion drawn in section 3.1.2.

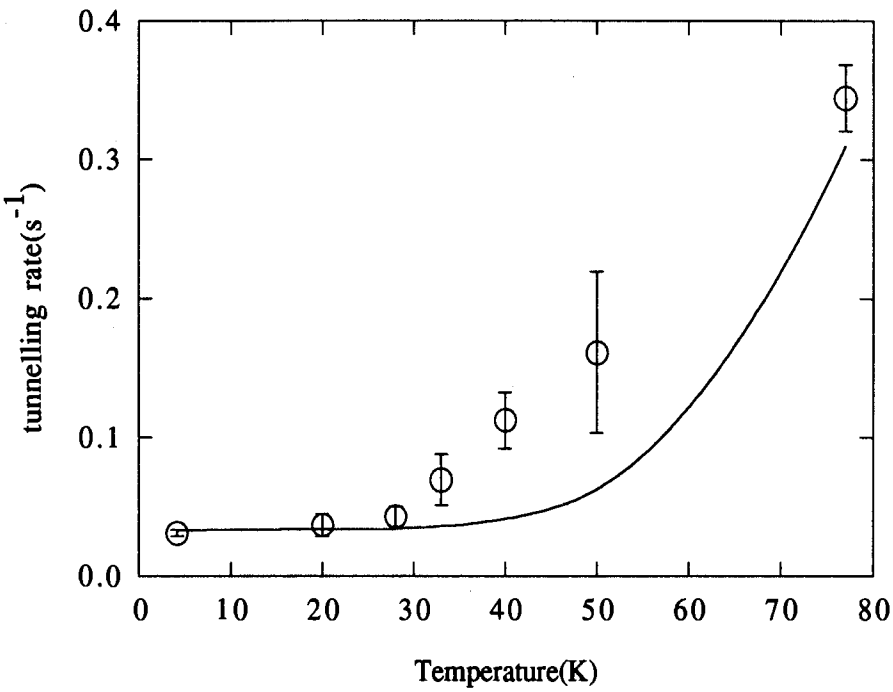

Figure 3.13 Temperature dependence of the bottleneck rate S. The scattering points are experimental value and the smooth curve is WKB approximation.

3.4 Summary and Conclusion

Quasiline fluorescence and excitation spectra of TBH_2Pc in *n*-alkane Shpol'skii matrices, especially in hexadecane, can be obtained by monochromatic excitation with a CW dye laser. These spectra reveal accurately the location of the molecular vibrational levels, which provides a necessary premise for the further investigation of intrinsic relaxation processes. A qualitative ball-and-stick model has been established to demonstrate the correlation between the chain length of the *n*-alkane and the quality of the Shpol'skii spectra, in this sense we found both theoretically and experimentally that hexadecane was the best Shpol'skii solvent. However, excitation and fluorescence spectra also indicated that the tighter the molecule fitted in the matrix, the greater was the molecular distortion.

TBH_2Pc in hexadecane system was chosen to illustrate the intramolecular photochemical reactions. The millisecond relaxation process, which is reflected by the reduction of fluorescence intensities after resonantly pumping, was directly observed. Our three-level model explained exceptionally well that this relaxation process originated from a metastable intermediate state. Such state was later identified as the lowest triplet state of the tautomer (1). The molecule first crossed from $S_1^{(2)}$ to $T_1^{(2)}$, where tautomer (2) transformed to tautomer (1), via vibronic coupling; then the millisecond process was a result of the transitions of $T_1^{(2)}$ to $S_0^{(1)}$. The characteristic time of this process ranged from 100 to 300 ms, depending on excitation power, but their was no experimental evidence to indicate its correlation with pumping state and initial ground state population. The average rate of this process was determined to be $(14.3\pm0.8)s^{-1}$.

Different fluorescence reductions caused by different dark times prior to the excitation revealed there existed a very slow dynamic process in TBH_2Pc. From the three-level model we learned that this process must follow the millisecond one, and we predicted it

be the result of concerted two-proton tunnelling through the molecular potential barrier in the ground state. This prediction agreed in general well with the numerical result from a WKB approximation at 0K. However, for the temperature dependence of this rate there was a rather large discrepancy with the theoretical calculation, which completely ignored the high degeneracy of the molecular vibrational levels. At the same time we do not exclude (1) that the mechanism may procede through single step proton tunnelling of the molecular potential and (2) that temperature may also change the molecular potential parameters.

It is also interesting to compare our proton tunnelling rate $(3.0\pm0.2)\times10^{-2}s^{-1}$ to the spectral hole recovery rate ($\sim2.6\times10^{-2}s^{-1}$) of TBH_2Pc in the same matrix derived by Haarer group[68]. This value is identical with ours within 10%. That is to say, the bottleneck effect is completely equivalent to the spectral hole-burning and the proton tunnelling rate is relevant to the persistence of the spectral hole. Permanent hole-burning offers potential technological applications for data storage in the frequency domain, as the presence of a hole at a particular frequency can be used to store a "bit" of information. From this point of view, TBH_2Pc imbedded in hexadecane may not be a good candidate for optical storage. However, initial experimental data in tunnelling rate that we acquired showed that TBH_2Pc in pentadecane and H_2Pc in octane-αClN mixture persisted even for hours. Therefore, although it seems early to conclude that (for the same molecule) less stress from the matrix may result in long tunnelling, or hole-burning, time, it has after all pointed a direction for the future hole-burning investigations.

REFERENCES

[1] N. Bloembergen, E.M. Purcell, R.V. Pound, Phys. Rev., **71,** 679(1948)

[2] A. Szabo, Phys. Rev. Lett., **25,** 924(1970)

[3] A. Szabo, Phys. Rev. **B11,** 4512(1975)

[4] B.M. Kharlamov, R.I. Personov, L.A. Bykovskaya, Opt. Comm., **12,** 191(1974)

[5] A.A. Gorokhovskii, R. Kaarli, L.A. Rebane, JETP Lett., **20,** 216(1974)

[6] S. Völker, J.H. Van der Waals, Mol. Phy. **32,** 1703(1976)

[7] I.E. Zalesski, V.N. Kotlo, A.N. Sevchenko, K.N. Solov'ev, S.F. Shkirman, Sov. Phys. Dokl. **17,** 1183(1973)

[8] K.N. Solov'ev, I.E. Zalesski, V.N. Kotlo, S.F. Shkirman, JETP Lett. **17,** 332(1973)

[9] W.E. Moerner, Proceedings of the International Conference '83, Ed. R.C. Powell, STS Press, 1983

[10] W.E. Moerner, M. Gehrtz, A.L. Huston, J. Phy. Chem., **88,** 6459(1984)

[11] L. Kador, G. Schulte, D. Haarer, J. Phys. Chem., **90,** 1264(1986)

[12] M. Romagnoli, W.E. Moerner, F.M. Schellenberg, M.D. Levenson, G.C. Bjorklund, J. Opt. Soc. Am., **B1,** 341(1984)

[13] W. Breinl, J. Freidrich, D. Haarer, J. Chem. Phys., **80,** 3496(1984)

[14] A.A. Gorokhovskii, V.V. Palm, JETP Lett., **37,** 201(1983)

[15] Th. Sesselmann, W. Richter, D. Haarer, J. Lum., **36,** 263(1987)

[16] A.P. Marchetti, M. Scozzava, R.H. Young, Chem. Phys. Lett., **51,** 424(1977)

[17] V.D. Samolilenko, N.V. Razumova, R.I. Personov, Opt. Spect., **52,** 346(1982)

[18] R.M. Macfarlane, R.M. Shelby, A. Winnacker, Phy. Rev., **B33,** 4207(1986)

[19] H. de Vries, D.A. Wiersma, Phys. Rev. Lett., **36,** 91(1976)

[20] D.M. Burland, D. Haarer, IBM J. Res. Devel., **23,** 534(1979)

[21] R.M. Hochstrasser, D.S. King, J. Am. Chem. Soc., **97,** 4760(1975)

[22] M. Iannone, G.W. Scott, D. Brinza, D.R. Coulter, J. Chem. Phys., **85,** 4863(1986)

[23] W. Breinl, J. Freidrich, D. Haarer, Phys. Rev., **B34,** 7271(1986)

[24] T. Tani, H. Namikawa, K. Arai, A. Makishima, J. Appl. Phys., **58,** 3559(1985)

[25] R.M. Macfarlane, R.M. Shelby, Phy. Rev. Lett., **42,** 788(1979)

[26] R.M. Macfarlane, R.M. Shelby, Opt. Lett., **9,** 533(1984)

[27] A. Winnacker, R.M. Shelby, R.M. Macfarlane, Opt. Lett., **10,** 350(1985)

[28] S. Völker, J. Lum., **36,** 251(1987)

[29] H.J. Meixner, A. Renn, S.E. Bucker, V.P. Wild, J. Phy. Chem., **90,** 6777(1986)

[30] A.A. Maradudin, "Theoretical and Experimental Aspects of the Effects of Points defects and Disorder on the Vibration of Crystals", Academic, 1966

[31] R.I. Personov, E.I. Al'shits, L.A. Bykovskaya, Opt. Comm., **6,** 169(1972)

[32] R.I. Personov, B.M. Kharmakov, Opt. Comm., **7,** 417(1973)

[33] L.A. Bykovskaya, R.I. Personov, B.M. Kharlamov, Chem. Phys. Lett., **27,** 80(1974)

[34] R.I. Personov, in "Spectroscopy and excitation Dynamics of Condensed Molecular Systems", Ed. V.M. Agranovich, R.M. Hochstrasser, North Holland, 1983

[35] R.I. Personov, Spectrochim. Acta **38B,** 1533(1983)

[36] É.V. Shpol'skii, Sov. Phys. Uspekhi, **3,** 372(1960)

[37] É.V. Shpol'skii, Sov. Phys. Uspekhi, **5,** 522(1962)

[38] É.V. Shpol'skii, Sov. Phys. Uspekhi, **6,** 411(1963)

[39] T.R. Koehler, J. Chem. Phys., **72,** 3389(1980)

[40] see, for example, S. Voelker, Chem. Phys. Lett. **87,** 481(1982)

[41] I.Y. Chan, W.G. van Dorp, T.J. Schaafsma, J.H. van der Waals, Mol. Phys., **22,** 741(1971)

[42] J.J. de Lange, J.M. Robertson, I. Woodward, Proc. Roy. Soc. London, **A171,** 398, 404(1939)

[43] B.F. Hoskins, S.A. Mason, J.C.B. White, J. Chem. Soc. (London) D 554(1969)

[44] NBS Monograph 125: Reference Tables for Thermocouples, 1974

[45] K. Burns, K.B. Adams, J. Longwell, J. Opt. Soc. Am. **40**, 339(1950)

[46] Th. Förster, K. Kasper, Z. Elektrochem. **59**, 976(1955)

[47] See, for example, S. Völker *et al*, J. Chem. Phys. **67**, 1759(1977)

[48] L. A. Rebane, A.A. Gorokhovskii, J.V. Kikas, Appl. Phys. **B29**, 235(1982)

[49] A.A. Gorokhovskii et al, Sov. Phys. Solid State, **19**, 1996(1977)

[50] J.L. Richards, S.A. Rice, J. Chem. Phys., **54**, 2014(1971)

[51] T.-H. Huang, K.E. Rieckhoff, E.-M. Voigt, J. Chem. Phys., **80**, 4051(1984)

[52] Y. Hu, MSc. thesis, Simon Fraser University, 1991

[53] M.J. Robertson, Organic Crystals and Molecules, Cornell University Press, 1953

[54] S. Voelker, R.M. Macfarlane, J. Chem. Phys., **73,** 4476(1980)

[55] S. Voelker, R.M. Macfarlane, IBM J. Res. Dev., **23,** 547(1979)

[56] R.M. Macfarlane, S. Voelker, Chem. Phys. Lett., **69,** 151(1980)

[57] G. Jansen, M. Noort, N. van Dijk, J.H. van der Waals, Mol. Phys., **39,** 865(1980)

[58] see, for example, W.G. van Dorp, T.J. Schaafsma, M. Soma, J.H. van der Waals, Chem. Phys. Lett., **21,** 47(1973)

[59] P.S.H. Fitch, C.A. Haynam, D.H. Levy, J. Chem. Phys., **73**, 1064(1980)

[60] W-H. Chen, K.E. Rieckhoff, E-M. Voigt, M.L.W. Thewalt, Molecular Phys., **67**, 1439(1989)

[61] K.-P. Müller, D. Haarer, Phys. Rev. Lett., **66,** 2344(1991)

[62] W-H. Chen, K.E. Rieckhoff, E-M. Voigt, Spectro. Acta, **46A,** 1801(1990)

[63] R.S. Becker, "Theory and Interpretation of Fluorescence and Phosphorescence", Wiley Intersciece, 1969

[64] A.T. Gradynshko, M.P. Tsvirko, Opt. Spectro., **31,** 291(1971)

[65] W.G. van Dorp, M. Soma, J.A. Kooter, J.H. van der Waals, Mol. Phys., **28,**1551 (1974)

[66] The standard WKB treatment can be found in many quantum mechanic textbook. See, for example, L.D. Landau, E.M. Lifshitz "Quantum Mechanics", Pergamon Press, 1977

[67] A. Ranfagni, G. Viliani, M. Cetica, G. Molesini, Phys. Rev., **B16,** (890)1977

[68] P. Geissinger, S. Reul, D. Haarer, K.E. Rieckhoff, Chem. Phys. Lett., **190,** 67(1992)